

FITTING A GALACTIC MODEL TO AN ALL-SKY SURVEY

JEFFREY A. LARSEN

Lunar and Planetary Laboratory, University of Arizona, 1629 East University Boulevard, Tucson, AZ 85721;
jlarsen@lpl.arizona.edu

AND

ROBERTA M. HUMPHREYS

Department of Astronomy, University of Minnesota, 116 Church Street, SE, Minneapolis, MN 55455;
roberta@aps.umn.edu

Received 2002 July 9; accepted 2003 January 2

ABSTRACT

We use star counts from the APS Catalog of the POSS I to develop a Galactic model optimized for large, statistically significant data sets uniformly distributed over the sky. The power of the APS Catalog for Galactic structure studies comes from its large sky coverage, individual photometric calibrations, adequate scanning resolution, statistically significant sample sizes, color information, and, most importantly, multidirectional sampling. The APS Catalog is an extremely useful exploratory data set but requires new methodologies to maximize its usefulness. We have selected an 88-field subset, 16 deg² each, from the catalog for a program of magnitude-limited star counts ($12 \leq O[\text{blue}] \leq 20$) within the completeness limit of the survey and in a realm where star-galaxy classification has minimal effects on the results. We have developed a simple three-component (disk, halo, thick disk) model optimized for efficiently and objectively analyzing star-count information. Our model not only produces model counts for our multidirectional data, but also returns a “goodness of fit” statistic. We use a *genetic algorithm*, a robust optimization technique well suited for this large multidirectional and multiple-parameter study, to optimize the fit and derive a self-consistent set of global parameters to model the Galaxy. With this global fit, we can identify significant deviations from symmetry in the Galaxy’s large-scale distribution of stars. The results from 12 independent executions or trials yielded consistent results. All of the model fits produced a flattened inner halo with $c/a \approx 0.5\text{--}0.6$. The radial scale length of the disk, ≈ 3.5 kpc, is higher than found in recent infrared surveys but agrees with older optical studies. The density normalizations to the plane for the thick disk and halo are consistent with previous work. Our model results all yielded a scale height for the thick disk of ≈ 900 pc. The most surprising results from these global fits are relatively high values (>4 kpc) for the de Vaucouleurs radius for the halo and the radial scale length of the thick disk. The radial scale length for the thick disk is significantly larger than that for the old/thin disk and, if confirmed with additional work, may imply an independent origin for the thick disk. We also present evidence that the scale height and normalization of the thick disk may be variable with direction.

Key words: Galaxy: fundamental parameters — Galaxy: structure — methods: data analysis — methods: statistical — surveys

1. INTRODUCTION

The method of star counts is one of the techniques of classical astronomy that has not yet exhausted its full potential. Modern work on star counts and Galactic structure was led by the development of high-speed, high-precision measuring machines such as APM, COSMOS, and the APS, which can rapidly and accurately digitize large-scale photographic plates. Although the initial focus of the early digitization programs was extragalactic, interest in the stellar data and Galactic studies was stimulated by the development of numerical models for the Galaxy that could be directly compared with the star counts. In these models, the forms of the stellar density distribution and luminosity function are adopted, and critical input parameters can be varied to achieve better agreement with the observations (see reviews by Bahcall 1986 and Gilmore, Wyse, & Kuijken 1989, plus the numerous references within).

Despite these important advances in technology and methodology, most Galactic structure studies using star counts have not taken full advantage of the potential to sample large areas of the sky to faint magnitudes. Many previous star-count studies have relied on data from several

sources with different filters and magnitude limits that covered different areas on the sky. Figure 1 in Bahcall (1986) illustrates this problem very clearly. But the primary limitation for many studies has been the small sky coverage, yielding data sets that are too small for statistically significant results. Another limitation to star-count studies over large areas of the sky has often been the lack of adequate photometric calibration to faint limiting magnitudes and a reliable, uniform system for object classification, essential for counts of both stars and galaxies. These problems very likely account for much of the variation found in the literature for key Galactic parameters. The APS Catalog of the POSS I provides a calibrated, uniform, and complete data set that can be sampled over three-fourths of the sky with accurate object classification to 20th magnitude, thus eliminating many of the statistical uncertainties.

Our previous studies with star counts from the APS Catalog illustrate what we can learn from sampling large areas on the sky in many different directions with a uniform data set. We used counts of faint blue stars from seven POSS fields, 16 deg² each, that included the north Galactic pole plus six others in the $l = 90^\circ/l = 270^\circ$ plane and derived an axial ratio $c/a \approx 0.6$ for the Galactic halo (Larsen &

Humphreys 1994). This flattened distribution remained even after the expected contribution from the thick disk was removed. In a different application (Humphreys & Larsen 1995), we compared the number of disk population stars in 12 Sky Survey fields (16 deg² each), six each at the north and south Galactic poles. The observed ratio led to a solar distance of 20.5 pc above the Galactic plane. Our most unexpected result was the discovery of a large asymmetry in the distribution of the faint blue stars at $b = 30^\circ$, with about 30% more stars in the $l = 20^\circ\text{--}45^\circ$ range as compared with the complementary longitudes on the other side of the Sun-center line (Larsen & Humphreys 1996). A more spatially complete study (Parker, Humphreys, & Larsen 2002, 2003) has confirmed this result. The excess in the star counts could be due to an interaction of the thick disk and inner halo stars with the stellar bar in the disk in the same direction (Weinberg 1992), or a possible triaxial thick disk or halo (Spergel 1992).

In this paper, we take full advantage of the APS Catalog—large spatial areas on the sky, individual photometric calibration for each field, object classification, and statistically significant sample sizes—to develop an optimized galaxy model based on star counts from 88 Sky Survey fields, 16 deg² each and uniformly distributed around the sky. A robust optimization routine, the *genetic algorithm*, well suited for this large multifield study, is applied to this large data set to derive a self-consistent set of parameters to model the Galaxy. Then, given this “all sky” model, we can search for statistically significant asymmetries and deviations in the star counts in different directions.

In the next section, we describe the observational data, the photometric calibration, the selection of the POSS fields, and their characteristics. In § 3, we present the Galactic model, GALMOD, and its formalization and input parameters. Section 4 includes a description of the genetic algorithm, and in § 5 we apply GALMOD with the genetic algorithm to the APS data with a series of test trials and independent executions on different sets of the data. In § 6, we discuss the results, comparisons with previous models, deviations from the best all-sky fit, and evidence for large-scale asymmetries. In the final section, we discuss possible improvements to the model and the applicability of genetic algorithms for modeling all-sky surveys.

2. OBSERVATIONS

The APS Catalog of the POSS I is derived from our scans of glass duplicate plates, blue (O) and red (E), of the original Palomar Observatory Sky Survey (POSS I). The POSS I plates are scanned in threshold densitometry mode. This scanning mode produces a single level of isodensity data at the threshold plus the actual pixel data above this threshold. The threshold is set at 65% of the background transmission, which is mapped on a flyback scan. Thus the densitometric data ($5\ \mu\text{m} \times 12\ \mu\text{m}$ pixels) are also available for all detected objects. Further information on the APS and its scanning procedures and parameters can be found in Pennington et al. (1993). The catalog¹ includes positions, magnitudes, colors, and star-galaxy classification, plus other image parameters for all matched objects on plate pairs with $|b| \geq 20^\circ$ and $\delta \geq -33^\circ$.

¹ The APS database is at <http://aps.umn.edu>.

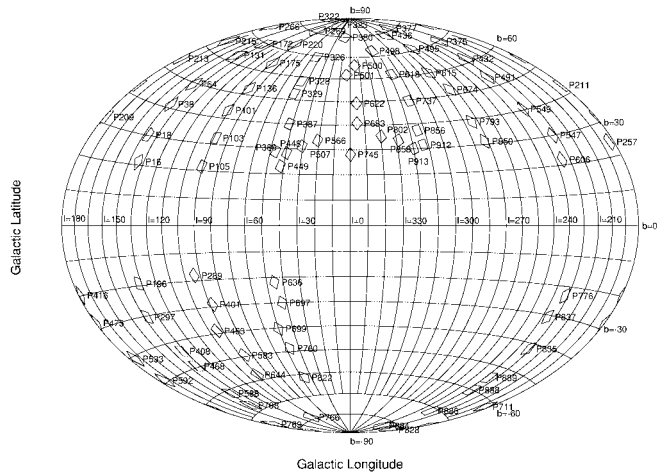


FIG. 1.—Aitoff projection showing the distribution of the 88 selected POSS fields around the Galactic sky.

For our Galactic model, we have selected 88 POSS I fields uniformly distributed around the sky at every 45° in longitude and every 10° in latitude for $|b| \geq 20^\circ$. The star-count data for the Galactic model are drawn from the central 16 deg² of each field, with a total of 2,524,740 stars between 12th and 20th magnitude on the 88 fields. Table 1 lists the 88 fields with the right ascension, declination, and Galactic longitude and latitude of the field centers and the source and magnitude limits of the photometric calibration. The distribution of these 88 fields on the sky is shown in Figure 1.

2.1. Photometric Calibration

APS data are photometrically calibrated with BVR_J photoelectric sequences from Kitt Peak (Humphreys et al. 1991) and CCD BVR_C sequences obtained at three different telescopes: the 0.6 m at the University of New Mexico’s Capilla Peak Observatory, the 0.76 m at the University of Texas McDonald Observatory, and the 0.9 m telescope at Cerro Tololo Inter-American Observatory. The observations were transformed to the standard system using published sequences in several open and globular clusters (Christian et al. 1985; Odewahn et al. 1992). Our calibrating sequences are all located near the centers of the POSS I plates and are available at the APS Web site. We also supplemented our sequences with data from the literature. The limiting magnitude of the sequences and the source or sources of the calibration for each field are included in Table 1.

When combined with the B and V photoelectric data of the Guide Star Photometric Catalog (GSPC; Lasker et al. 1988) for the brighter stars, we have direct calibration from approximately 10th to 21st magnitude for the blue plates and 13th to 20th magnitude on the red plates. The magnitudes on the standard system are transformed to the instrumental (emulsion plus filter system) O (blue) and E (red) passbands of the Sky Survey plates (see Humphreys et al. 1991). For a few fields in which only GSPC photometry was available, there were no R -band magnitudes for the red (E) transformation. To supplement these data, we derived a relation between $B-V$ and $V-R_C$ from the Landolt standards (Landolt 1992) that is linear for $B-V \leq 1.3$. With this relation, an R magnitude can be derived from the GSPC B and V photometry and transformed to our E passband.

TABLE 1
DIRECTION AND CALIBRATION INFORMATION FOR THE APS GALACTIC STRUCTURE FIELDS

| APS FIELD | PLATE CENTER (B1950.0) | | | | $E(B-V)^a$ | PHOTOMETRY | | O COMPL. |
|--------------|------------------------|-------------|-----------|-----------|------------|---------------------|------------|-------------|
| | R.A. | Decl. | l (deg) | b (deg) | | Source ^b | O/E Calib. | |
| P16..... | 04 50 44.00 | +78 09 05.0 | 134.0 | 21.1 | 0.13 | 1, 2 | 20.5/19.1 | 19.5 |
| P18..... | 07 53 36.00 | +77 45 44.0 | 136.6 | 30.1 | 0.04 | 1, 2 | 21.8/19.5 | 20.0 |
| P38..... | 10 19 34.00 | +71 31 16.0 | 137.8 | 41.3 | 0.04 | 1, 2 | 19.7/19.1 | 20.0 |
| P64..... | 11 21 41.00 | +65 28 45.0 | 136.8 | 49.5 | 0.01 | 1, 2 | 19.5/18.4 | 20.0 |
| P101..... | 16 09 37.00 | +59 45 10.0 | 91.0 | 43.2 | 0.03 | 1, 2 | 20.5/18.8 | 20.0 |
| P103..... | 17 37 16.00 | +59 57 01.0 | 88.7 | 32.4 | 0.05 | 1, 2 | 21.8/19.9 | 20.0 |
| P105..... | 19 05 21.00 | +60 08 51.0 | 90.7 | 21.6 | 0.10 | 1, 2 | 20.9/19.7 | 19.5 |
| P131..... | 12 06 42.00 | +53 28 16.0 | 136.8 | 62.8 | 0.00 | 1, 2 | 19.3/18.1 | 18.5 |
| P136..... | 15 14 41.00 | +53 38 54.0 | 87.6 | 52.6 | 0.01 | 1, 2 | 19.8/18.5 | 20.0 |
| P172..... | 12 32 33.00 | +47 28 33.0 | 131.0 | 69.7 | 0.00 | 1 | 16.2/ ... | 20.0 |
| P175..... | 14 13 37.00 | +47 33 23.0 | 89.3 | 63.9 | 0.01 | 1, 2 | 21.8/19.9 | 20.0 |
| P196..... | 01 35 38.00 | +42 29 13.0 | 132.1 | -19.3 | 0.11 | 1, 2 | 21.0/19.2 | 19.5 |
| P209..... | 08 06 29.00 | +41 43 31.0 | 178.9 | 31.7 | 0.06 | 1 | 15.7/ ... | 20.0 |
| P211..... | 09 06 10.00 | +41 37 13.0 | 180.3 | 42.8 | 0.00 | 1, 2 | 20.9/18.5 | 20.0 |
| P213..... | 10 05 47.00 | +41 32 10.0 | 179.2 | 53.9 | 0.00 | 1, 2 | 20.2/19.0 | 20.0 |
| P215..... | 11 05 20.00 | +41 29 17.0 | 172.7 | 64.6 | 0.00 | 1, 2 | 21.1/18.6 | 20.0 |
| P220..... | 13 34 07.00 | +41 30 54.0 | 92.7 | 73.1 | 0.00 | 1, 2 | 19.9/19.3 | 20.0 |
| P257..... | 07 34 17.00 | +35 47 39.0 | 183.7 | 24.2 | 0.07 | 1, 2 | 21.5/19.4 | 20.0 |
| P266..... | 11 44 58.00 | +35 28 20.0 | 178.4 | 74.2 | 0.00 | 1, 2 | 16.6/18.1 | 20.0 |
| P269..... | 13 08 26.00 | +35 29 27.0 | 97.1 | 80.9 | 0.00 | 1, 2, 3 | 22.7/20.4 | 20.0 |
| P289..... | 22 28 15.01 | +36 29 07.0 | 93.8 | -18.0 | 0.17 | 1, 2 | 21.5/20.3 | 19.5 |
| P297..... | 01 49 25.00 | +30 28 25.0 | 138.1 | -30.4 | 0.05 | 1, 2 | 20.7/19.5 | 19.0 |
| P322..... | 12 38 40.00 | +29 28 42.0 | 169.9 | 86.9 | 0.02 | 1, 2 | 21.4/19.2 | 20.0 |
| P323..... | 13 04 33.00 | +29 29 25.0 | 65.4 | 86.0 | 0.01 | 1, 2, 4, 5 | 21.7/19.4 | 20.0 |
| P326..... | 14 22 08.00 | +29 34 26.0 | 44.6 | 69.5 | 0.00 | 1, 2 | 22.0/20.0 | 20.0 |
| P328..... | 15 13 59.00 | +29 38 40.0 | 45.8 | 58.2 | 0.01 | 1, 2 | 19.4/18.2 | 20.0 |
| P329..... | 15 39 52.00 | +29 41 41.0 | 46.9 | 52.6 | 0.02 | 1, 2 | 20.1/18.8 | 20.0 |
| P375..... | 11 21 01.00 | +23 28 43.0 | 219.3 | 69.8 | 0.00 | 1 | 15.5/ ... | 20.0 |
| P377..... | 12 12 50.00 | +23 28 17.0 | 236.7 | 80.9 | 0.02 | 1, 2, 4 | 21.6/19.6 | 20.0 |
| P380..... | 13 30 31.00 | +23 30 35.0 | 12.8 | 79.9 | 0.00 | 1, 6 | 15.5/15.0 | 20.0 |
| P387..... | 16 32 00.00 | +23 47 45.0 | 42.1 | 40.0 | 0.04 | 1, 2 | 20.4/18.6 | 20.0 |
| P389..... | 17 23 58.00 | +23 54 51.0 | 46.7 | 28.7 | 0.09 | 1, 2 | 22.4/17.7 | 20.0 |
| P401..... | 22 36 31.00 | +24 29 36.0 | 88.3 | -29.1 | 0.06 | 1, 2 | 21.5/19.9 | 19.5 |
| P408..... | 01 17 05.00 | +18 30 06.0 | 132.2 | -43.6 | 0.04 | 1, 2 | 19.9/19.1 | 18.5 |
| P416..... | 04 29 30.00 | +18 12 16.0 | 178.9 | -19.8 | 0.40 | 1, 2 | 21.2/19.7 | 19.0 |
| P432..... | 10 53 04.00 | +17 29 37.0 | 227.2 | 61.5 | 0.01 | 1, 2 | 21.4/19.3 | 20.0 |
| P436..... | 12 28 47.00 | +17 28 30.0 | 276.8 | 79.0 | 0.01 | 1, 2 | 21.4/19.4 | 20.0 |
| P448..... | 17 16 11.00 | +17 53 52.0 | 39.5 | 28.3 | 0.10 | 1 | 15.2/ ... | 19.0 |
| P449..... | 17 40 14.00 | +17 57 08.0 | 42.0 | 23.0 | 0.11 | 1, 4 | 19.5/16.2 | 20.0 |
| P463..... | 23 16 44.00 | +18 31 08.0 | 94.5 | -38.9 | 0.04 | 1, 2 | 21.5/19.5 | 18.5 |
| P468..... | 01 17 01.00 | +12 30 00.0 | 133.6 | -49.5 | 0.03 | 1, 2 | 20.3/19.9 | 18.0 |
| P475..... | 04 05 16.00 | +12 15 32.0 | 179.8 | -28.1 | 0.30 | 1, 2 | 20.1/18.2 | 18.0 |
| P491..... | 10 29 05.00 | +11 30 30.0 | 231.9 | 53.6 | 0.03 | 1, 2 | 20.9/19.4 | 20.0 |
| P495..... | 12 04 49.00 | +11 27 15.0 | 267.8 | 71.0 | 0.00 | 1 | 16.7/ ... | 20.0 |
| P498..... | 13 16 43.00 | +11 29 55.0 | 326.6 | 72.8 | 0.00 | 1, 3 | 21.4/20.5 | 20.0 |
| P500..... | 14 04 39.00 | +11 32 24.0 | 354.9 | 66.2 | 0.00 | 1, 2 | 20.7/19.2 | 20.0 |
| P501..... | 14 28 36.00 | +11 34 47.0 | 3.8 | 61.8 | 0.01 | 1, 2 | 21.4/19.7 | 20.0 |
| P507..... | 16 52 29.00 | +11 50 22.0 | 30.5 | 31.2 | 0.08 | 1, 3 | 20.6/20.5 | 20.0 |
| P533..... | 03 17 02.00 | +06 20 49.0 | 175.2 | -40.8 | 0.20 | 1, 2 | 21.6/19.9 | 19.5 |
| P547..... | 08 53 02.00 | +05 38 25.0 | 222.9 | 30.0 | 0.05 | 1, 2 | 21.4/19.4 | 20.0 |
| P549..... | 09 41 02.00 | +05 33 49.0 | 230.3 | 40.3 | 0.02 | 1, 2 | 21.9/19.8 | 20.0 |
| P566..... | 16 28 40.00 | +05 47 42.0 | 21.0 | 33.7 | 0.09 | 1, 3 | 20.7/20.5 | 20.0 |
| P583..... | 23 16 49.00 | +06 31 11.0 | 86.3 | -49.4 | 0.06 | 1, 2 | 21.3/19.1 | 19.5 |
| P588..... | 01 16 52.00 | +00 30 02.0 | 137.6 | -61.3 | 0.02 | 1, 2, 7 | 21.4/18.7 | 18.5 |
| P592..... | 02 52 52.00 | +00 23 10.0 | 175.1 | -49.3 | 0.07 | 1, 2, 7 | 21.5/20.4 | 19.0 |
| P606..... | 08 28 52.00 | -00 19 12.0 | 225.4 | 21.8 | 0.04 | 1, 7 | 21.3/19.7 | 20.0 |
| P615..... | 12 04 52.00 | -00 31 44.0 | 280.4 | 60.1 | 0.01 | 1, 7 | 15.7/ ... | 20.0 |
| P618..... | 13 16 49.00 | -00 22 50.0 | 317.7 | 61.4 | 0.01 | 1, 2, 7 | 21.8/20.0 | 20.0 |
| P622..... | 14 52 52.00 | -00 23 17.0 | 355.1 | 49.3 | 0.05 | 1, 2, 7 | 21.3/19.5 | 20.0 |
| P636..... | 20 28 52.00 | +00 19 07.0 | 45.4 | -21.8 | 0.15 | 1, 7 | 21.6/20.2 | 19.0 |
| P644..... | 23 40 52.00 | +00 31 38.0 | 89.8 | -57.6 | 0.04 | 1, 2, 7 | 20.4/20.0 | 19.5 |
| P674..... | 11 40 51.00 | -06 31 38.0 | 274.6 | 52.3 | 0.03 | 1, 2, 7 | 21.2/19.5 | 20.0 |
| P683..... | 15 17 03.00 | -06 20 35.0 | 355.2 | 40.8 | 0.09 | 1, 2, 7 | 21.5/19.4 | 20.0 |

TABLE 1—Continued

| APS FIELD | PLATE CENTER (B1950.0) | | | | $E(B-V)^a$ | PHOTOMETRY | | O COMPL. |
|--------------|------------------------|-------------|-----------|-----------|------------|---------------------|------------|-------------|
| | R.A. | Decl. | l (deg) | b (deg) | | Source ^b | O/E Calib. | |
| P697..... | 20 53 01.00 | -05 38 20.0 | 42.9 | -30.0 | 0.06 | 1, 7 | 20.0/20.1 | 19.5 |
| P699..... | 21 40 58.99 | -05 34 01.0 | 50.3 | -40.3 | 0.03 | 1, 7 | 21.7/20.4 | 19.5 |
| P708..... | 01 16 48.00 | -05 30 02.0 | 141.0 | -67.1 | 0.03 | 1, 7 | 15.3/ ... | 19.0 |
| P711..... | 02 28 36.00 | -11 34 34.0 | 183.8 | -61.8 | 0.01 | 1, 7 | 20.9/19.8 | 19.5 |
| P737..... | 13 17 01.00 | -12 30 00.0 | 313.6 | 49.5 | 0.02 | 1, 4 | 21.7/21.1 | 20.0 |
| P745..... | 16 05 17.00 | -12 15 19.0 | 359.8 | 28.1 | 0.33 | 1 | 15.4/ ... | 20.0 |
| P760..... | 22 05 48.01 | -11 32 07.0 | 47.4 | -48.6 | 0.03 | 1, 7 | 20.8/20.4 | 19.0 |
| P766..... | 00 28 47.00 | -17 28 31.0 | 96.8 | -79.0 | 0.02 | 1, 7 | 21.2/21.1 | 18.5 |
| P769..... | 01 40 35.00 | -17 31 12.0 | 176.0 | -74.5 | 0.00 | 1, 7 | 19.9/20.7 | 18.5 |
| P776..... | 05 40 12.00 | -17 57 13.0 | 222.0 | -23.1 | 0.02 | 1, 7 | 15.9/ ... | 17.0 |
| P793..... | 11 16 44.00 | -18 31 12.0 | 274.5 | 38.9 | 0.04 | 1, 7 | 18.8/19.6 | 20.0 |
| P802..... | 14 52 22.00 | -18 23 06.0 | 339.6 | 35.3 | 0.12 | 1 | 15.4/ ... | 20.0 |
| P822..... | 22 53 04.00 | -17 29 37.0 | 47.2 | -61.5 | 0.02 | 1, 7 | 21.0/20.1 | 18.5 |
| P828..... | 01 21 35.00 | -23 36 32.0 | 187.5 | -81.7 | 0.02 | 1, 7 | 19.6/17.4 | 18.5 |
| P835..... | 04 23 09.00 | -23 49 51.0 | 221.4 | -42.0 | 0.02 | 1, 7 | 21.2/19.5 | 18.5 |
| P837..... | 05 15 07.00 | -23 56 06.0 | 225.9 | -30.7 | 0.01 | 1, 7 | 19.7/18.8 | 18.5 |
| P850..... | 10 53 37.00 | -24 23 57.0 | 272.1 | 31.2 | 0.09 | 1, 7 | 20.1/18.8 | 20.0 |
| P856..... | 13 30 08.00 | -24 23 10.0 | 314.8 | 37.3 | 0.09 | 1, 7 | 20.5/19.3 | 19.0 |
| P858..... | 14 22 17.00 | -24 20 27.0 | 328.7 | 33.6 | 0.10 | 1 | 14.4/ ... | 20.0 |
| P884..... | 01 19 52.00 | -29 41 20.0 | 233.5 | -82.8 | 0.01 | 1, 8 | 20.5/18.1 | 18.5 |
| P886..... | 02 13 19.00 | -29 39 00.0 | 224.9 | -71.4 | 0.00 | 1, 7 | 16.4/18.2 | 19.0 |
| P888..... | 03 05 10.00 | -29 42 32.0 | 225.6 | -60.1 | 0.00 | 1, 7 | 20.1/18.0 | 18.5 |
| P889..... | 03 31 04.00 | -29 44 47.0 | 226.6 | -54.5 | 0.00 | 1, 7 | 17.4/18.9 | 18.5 |
| P912..... | 13 30 13.00 | -30 23 13.0 | 313.4 | 31.4 | 0.05 | 1, 7 | 20.8/19.7 | 19.0 |
| P913..... | 13 56 19.00 | -30 21 59.0 | 319.8 | 30.0 | 0.07 | 1 | 14.9/ ... | 19.5 |

NOTE.—Units of right ascension are hours, minutes, and seconds, and units of declination are degrees, arcminutes, and arcseconds.

^a As determined over field from the maps of Burstein & Heiles 1982.

^b Sources of calibration: (1) photoelectric photometry from the Guide Star Photometric Catalog (Lasker et al. 1988); (2) CCD photometry from Capilla Peak; (3) CCD photometry from McDonald Observatory; (4) photoelectric photometry from Humphreys et al. 1991; (6) unpublished photoelectric photometry from M. Postman & E. Siciliano (1992); (7) CCD photometry from CTIO; (5) CCD photometry from S. R. Majewski (1993, private communication); (8) ESO/SERC CCD calibration for field 412 (Cunow 1993).

We then derive a magnitude-diameter relation in each color for each field from the calibrating sequences and the diameters of the best-fit ellipses for the corresponding stellar images on the plates. The resulting relation is fitted by a smooth function based on the stellar brightness profile of the image (see King 1971; Kormendy 1973). Figure 2 shows a sample magnitude-diameter fit. The rms of the calibrations is typically 0.15 mag for the magnitude range $O = 15-20$, with expected zero-point errors of 0.02–0.10 mag. The majority of instances in which the error in the $O-E$ color exceeds 0.1 mag are due to the lack of reliable calibration fainter than 15th magnitude. A sample color-magnitude diagram, O magnitude versus $O-E$ color, is shown in Figure 3. For a quick conversion, the $O-E$ color is approximately 1.7 times the $B-V$ color, except for the reddest stars. The completeness limit for each of the O -band plates is also included in Table 1. This limit is always brighter than the limiting magnitude on the O plate and is caused primarily by blue stars whose E magnitude is fainter than the red-plate limit (see Fig. 3).

2.2. Interstellar Reddening Correction

While interstellar extinction is small for most of our fields, it can be significant, especially for the fields below $|b| = 30^\circ$. For this reason, we obtain the mean reddening $E(B-V)$, from the Burstein & Heiles (1982) maps, in the central 16 deg² region we are using for the star counts. The mean value

for each POSS I field is given in Table 1. They are transformed to our color system [A_O and $E(O-E)$] using the standard extinction law. Since the completion of this initial work, improved extinction maps by Schlegel, Finkbeiner, & Davis (1998) with better spatial resolution have become available. In Figure 4, we compare the average difference in the extinction for our 88 fields from the two surveys. Except

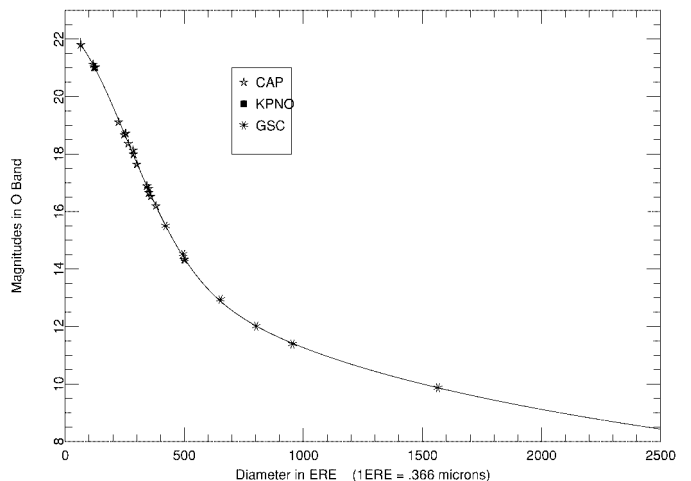


FIG. 2.—A magnitude-diameter calibration fit from POSS plate P103

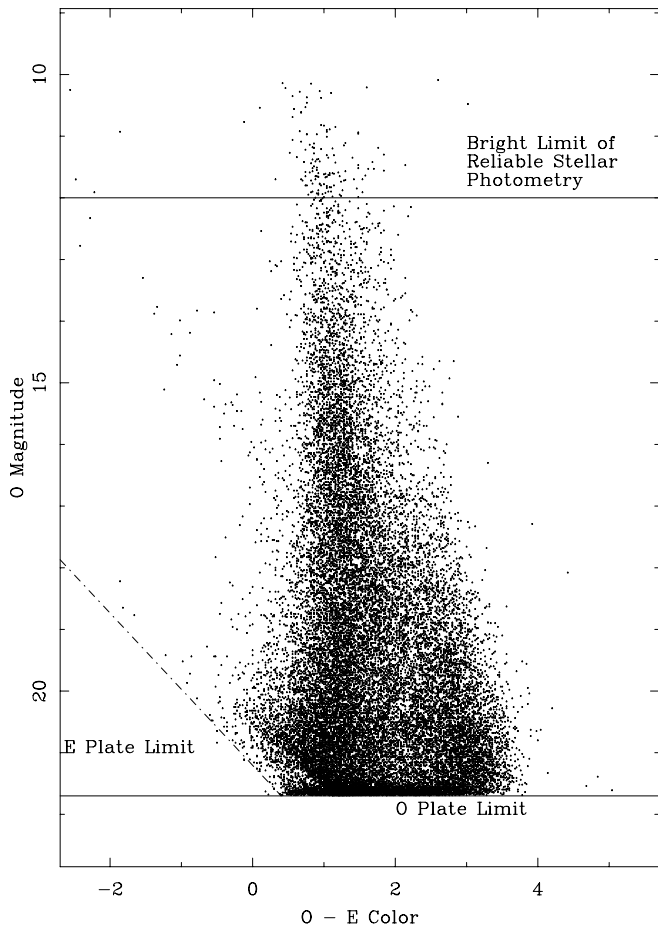


FIG. 3.—Sample color-magnitude diagram (P323, the north Galactic pole).

at the lowest Galactic latitudes, the differences between the two surveys are smaller than the individual photometric zero-point systematics (§ 2.4). Since the errors from using the newer work simply increase the magnitude of the corrections

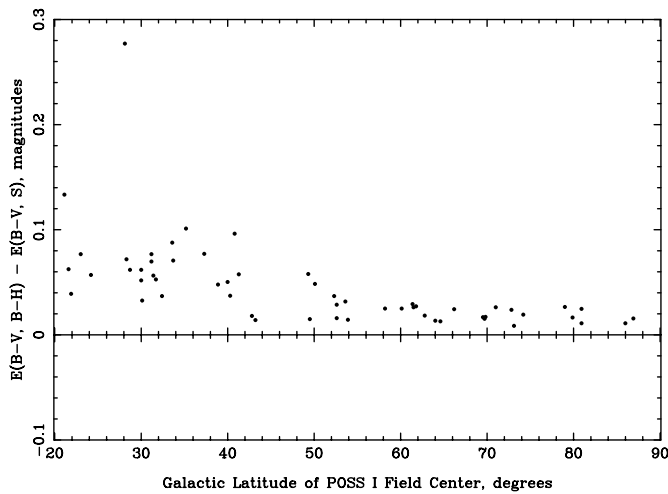


FIG. 4.—Comparison of the extinction estimates over our survey regions between Schlegel et al. [1998; $E(B-V, S)$] and Burstein & Heiles [1982; $E(B-V, B-H)$]. Note that while systematic differences exist for all except the lowest latitude fields, the magnitude of the differences is small.

discussed in § 2.4, we continue to use our original results from the Burstein & Heiles maps, although any future work will be done with the Schlegel et al. data.

2.3. Object Classification

The accurate separation of stellar and nonstellar images in any digitized or digital database is critical for both Galactic and extragalactic studies. However, the automated classification of objects is a difficult problem. In the APS Catalog, the stellar and nonstellar images are separated with a neural network-based classifier developed by Odewahn et al. (1992, 1993). The neural network uses various image parameters with a back-propagation algorithm and two hidden layers to generate an output layer with two nodes, star and nonstar (i.e., “galaxy”). The classifier has a success rate of better than 90% for galaxies to $O \approx 19.5-20.0$ mag at the higher Galactic latitudes, and better than 98% for stars overall.

2.4. Internal Systematics: Blended Images and the Zero Point

Blended star-star images are not stellar and therefore are often labeled nonstellar or “galaxy” by our automated classifier. This is primarily a problem for plates near the Galactic plane or center, where the increasing density of images produces more blends (see Fig. 5). While this is a normalization problem, it primarily affects the low-latitude plates.²

For the purposes of this study, we apply a statistical correction to the star counts for the expected number of blended images that depends on the density of stars. We first define a threshold number of galaxies above which the excess galaxies are very likely blended stars. For 15 fields at the north Galactic cap, the mean number of galaxies with diameters in the stellar magnitude range $12 < O < 20$ is 4234 with a standard deviation of 1165. While visual examination of the images shows that a very small fraction of

² A morphological classifier for galaxies is presently being developed for the APS database and includes a blended image class, which will remove the star-star blends and multiple images from the galaxy class.

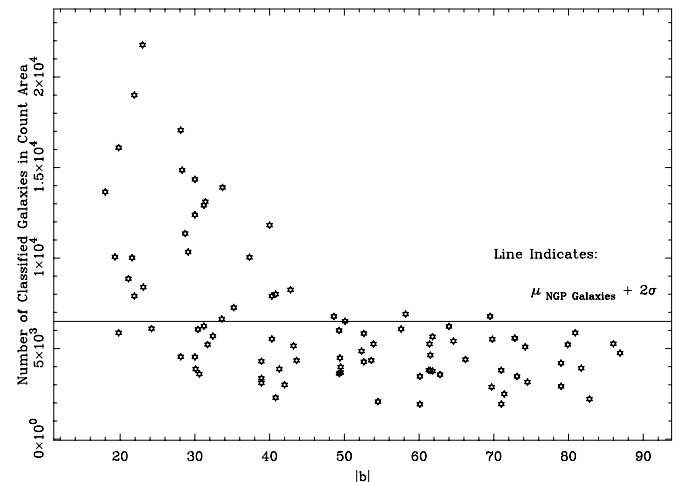


FIG. 5.—Distribution of APS-classified “galaxies” as a function of Galactic latitude, showing the inclusion of merged stars at lower latitudes.

these galaxies are also blends, the overall effect of blended images at the cap is small. We then define a threshold number of galaxies to be 2σ above the mean, or approximately 6500 galaxies. This gives a 97% confidence that fields with more than 6500 classified galaxies are contaminated by blended images. The number of merged stars is then twice the amount of galaxies in excess of 6500. This threshold is indicated on Figure 5. Once we have estimated the number of blended stars, we must now “reintroduce” them into their respective color-magnitude relations for the field.

To determine the correction as a function of magnitude, we used two representative fields, one at the north Galactic pole and one near the Galactic plane. Knowing the area surveyed, we can find the total area occupied by stars in each field, and then using mean free path arguments from classical physics, we can add stars of various diameters and predict the chance that they will end up in blended images. The distribution of blended images with diameter is roughly the same percentage for both fields (both still contain a respectable amount of blank sky), so we adopt the mean of the two for our correction. These additional stars are then added to each field as a function of magnitude and according to the observed color distribution. For our two test fields, this method introduces at most an error of 30% in how the stars are reintroduced. Since the blended images are approximately 15% of the total sample, the net error introduced by the correction is at most 5% and preferentially affects the low-latitude fields.

Zero-point errors in the photometric calibrations can also introduce systematic errors in our colors of 0.1–0.2 mag. We want to use impartial statistical techniques (such as χ^2) to determine the goodness of fit, which would be greatly biased by ± 0.2 mag or greater error in the color. To correct for this, we used a clearly identifiable feature on all of the color-magnitude diagrams, the peak of the blue ridge in the color-magnitude diagrams (see Fig. 3), which usually occurs near an O–E color of 1.0 for the POSS fields with low interstellar reddening. Assuming that this peak will occur in the color range $1.0 < \text{O–E} < 1.2$, we have shifted all of the observed color distributions, after correction for interstellar extinction, so that the peak color occurs in this range. So in effect, *we have put all of the fields on the same photometric system to within ± 0.1 mag.*

2.5. The Role of Binaries

With 50% or more of all known disk stars expected to be binary or multiple, unresolved binaries could have a significant effect on the derived stellar densities and scale heights in a Galactic model. In a recent paper, Siegel et al. (2002) show that ignoring binaries can steepen the density law and reduce the derived scale height. Using the *Hubble Space Telescope (HST)* Snapshot Survey, Gould et al. (1995) found that about 4% of the old disk stars with heights 500–1500 pc have companions with separations in the range $0''.13$ – $4''.0$, although the fraction of binaries in the thick disk and halo is not known. With our scanning resolution of $5\ \mu\text{m}$ ($0''.33$), combined with the resolution of the photographic plates ($25\ \mu\text{m}$) and the typical seeing disk of $2''$ – $3''$, stars with separations between $\sim 1''$ and $\sim 3''$ will appear as blended images in our scans. Thus, these wide binaries will be largely accounted for with our blended-image correction described above. Previous work did not correct for binaries, and consequently we have chosen not to apply any

additional corrections, especially given the uncertainty of binaries in the thick disk and halo.

2.6. Potential Contamination by Quasars, White Dwarfs, and Misclassified Galaxies

Our star counts will include contamination by non-main-sequence stars (i.e., white dwarfs) and extragalactic sources such as quasars and misclassified galaxies. At the poles, direct integration of the white dwarf luminosity functions of Fleming, Liebert, & Green (1986) and Liebert, Dahn, & Monet (1988) predicts that white dwarfs will have an areal density of approximately five per square degree (of which four will appear in the range $19 < \text{O} < 20$). Examination of the O–E colors for white dwarfs measured by Evans (1992) shows that the overwhelming majority are bluer than O–E = 0.6. At the poles, white dwarfs would represent only about 10% of the bluest tail of the distribution in our faintest magnitude bin, and so we can neglect them in this analysis.

Reid & Majewski (1993) caution that at $V \approx 20.5$, 25% of all blue starlike objects are quasars or compact narrow emission line galaxies. High-redshift quasars (those having $2.2 < z < 3.3$) are very rare. The cumulative quasar surface estimates of Hartwick & Schade (1990) indicate only two high-redshift quasars per square degree to $B = 20$. The corresponding O–E colors for these quasars, in an optically selected sample, are expected to range from 1 to 1.5 mag (McMahon 1991). These quasars are lost in the stellar distributions and contaminate the polar counts by only 1% and at lower latitudes by only 0.1%. For lower redshift quasars (those with $0 < z < 2.2$), Hartwick & Schade predict approximately 16 quasars per square degree down to $B = 20$. The distribution of these quasar colors peaks bluer than the canonical halo turnoff color of $B - V \approx 0.6$. These quasars will constitute 18% of the polar halo stars bluer than O–E ≈ 1.0 in the faintest magnitude bin. For the very bluest objects, O–E ≤ 0.6 , the quasars constitute 25% of the total number of polar stars. These fractions reduce to 5% and 12%, respectively, at lower latitudes. Since quasars are presumably distributed isotropically across the sky, they will therefore bias the models toward choosing a rounder distribution for the halo.

Besides blended images, there are still possible errors in the star-galaxy classification. As one looks to fainter and fainter magnitudes, the number of stars seen will eventually decrease to zero, while the number of galaxies will continue to increase. The numbers of stars and galaxies become comparable to one another at $J = 20.5$ – 21.5 mag (Jarvis & Tyson 1981; Koo & Kron 1982), which is significantly fainter than our cutoff at 20th magnitude. In fields near the Galactic poles, the ratio of stars to galaxies in our last magnitude bin, $19 < \text{O} < 20$, is about 2.5:1, and brighter than O = 18 the number of galaxies is negligible, as expected from other studies.

Therefore, discounting blends, misclassification is not a critical effect for the stellar distributions down to O = 20. Galaxies misclassified as stars will not significantly affect the star sample, as there are so few galaxies compared with stars in all of our magnitude ranges. With a 98% success rate for classifying stars, the number of stars misclassified as galaxies is also small. The principal concern from misclassification is not the effect on our star counts but, instead, the

contamination of the numerically smaller galaxy class by stars.

3. THE GALACTIC MODEL

We have designed a Galactic model called GALMOD specifically for use with our multidirectional star counts and optimized for efficiency. It has been heavily influenced by the models of Bahcall & Soneira (1980) and G. F. Gilmore (1995, private communication). The design is deliberately simple to avoid modeling the Galaxy at a level of detail not in our data. Our basic design philosophy has been to use previous Galactic model information for the three major stellar populations in the Galaxy—the disk, halo, and thick disk—and to concentrate on studying their global spatial distribution. The mathematical formulation, the adopted luminosity function, and the color-magnitude relation for each component are summarized in Table 2. For comparison with the previous work, we have adopted the standard or classical formulation used in those studies (Bahcall & Soneira 1980; G. F. Gilmore 1995, private communication).

3.1. The Disk

De Vaucouleurs (1959) studied the shapes of disks in spiral galaxies using their integrated light profiles and concluded that their light distribution is well described by a double exponential in R , the distance from the center, and Z , the distance above or below the plane. De Vaucouleurs' analysis started a long tradition of using the double exponential to represent the Galaxy's disk. Unfortunately, an

exponential density function has no dynamical basis—it is merely a convenient fitting function. In a truly physical model, the disk density function could be represented by an isothermal sech² distribution (van der Kruit & Searle 1982; Reid & Majewski 1993). However, for comparison with previous work and for computational simplicity, we continue with an exponential function, defined by

$$D(r) = N_{0,\text{disk}} \exp \left(\frac{-|Z - Z_\odot|}{Z_{H,\text{disk}}} - \frac{|R - R_\odot|}{R_{H,\text{disk}}} \right),$$

where $N_{0,\text{disk}}$ is the normalization of the disk to the disk density in the solar neighborhood, Z_\odot and R_\odot are the Sun's position, and $Z_{H,\text{disk}}$ and $R_{H,\text{disk}}$ are the scale lengths of the double exponential. The quantity $N_{0,\text{disk}}$ should be 1.00 if the solar neighborhood density is representative of the disk as a whole.

An additional complication to the density function is that vertical velocity dispersions are a function of age (and, hence, absolute magnitude). Stars are essentially born directly in the midplane of the disk out of large clouds of dust and gas. Usually, these stars form in groups but are torn apart over time by gravitational interactions with other clouds and stars, and the stars' vertical motions generally increase in amplitude after these interactions. If all stars lived to equal ages, all would be affected equally. However, the brightest stars do not live as long as the fainter stars and, so, on average are found closer to the plane. The quantity $Z_{H,\text{disk}}$ is therefore a function of age and absolute magnitude [or $Z_{H,\text{disk}}(M)$]. To account for this effect, we have adopted Gilmore's (1981) relation for dwarf scale heights. The most

TABLE 2
FEATURES OF GALMOD STAR-COUNT MODEL

| Quantity | Description |
|--------------------------------|--|
| Disk | |
| Density | $D(r) = N_{0,\text{disk}} \exp ([- Z /Z_{H,\text{disk}}] + [-(R - R_\odot)/R_{H,\text{disk}}])$ |
| Parameters: | |
| $N_{0,\text{disk}}$ | Normalization of disk density to luminosity function |
| $Z_{H,\text{disk}}$ | Vertical scale height of stars in the disk |
| R_\odot | Solar distance in midplane from the Galactic center |
| $R_{H,\text{disk}}$ | Radial scale length of the Galactic disk |
| Luminosity function | From Gilmore model; see text |
| Color-magnitude relation | From Gilmore model; see text |
| Thick Disk | |
| Density | $D(r) = N_{0,\text{thick}} \exp ([- Z /Z_{H,\text{thick}}] + [-(R - R_\odot)/R_{H,\text{thick}}])$ |
| Parameters: | |
| $N_{0,\text{thick}}$ | Normalization of thick disk density to disk |
| $Z_{H,\text{thick}}$ | Vertical scale height of stars in the thick disk |
| R_\odot | Solar distance from the Galactic center in the plane |
| $R_{H,\text{thick}}$ | Radial scale length of the thick disk |
| Luminosity function | From Gilmore model |
| Color-magnitude relation | 47 Tuc from Gilmore model |
| Halo | |
| Density | $N_{\text{halo}}(R'/r_e)^{7/8} \exp [-7.669(R'/r_e)^{1/4}]$ |
| Parameters: | |
| N_{halo} | Normalization of halo density to that of the disk |
| r_e | "De Vaucouleurs radius" |
| R' | $(R^2 + [(c/a)Z]^2)^{1/2}$ |
| Luminosity function | From Gilmore model |
| Color-magnitude relation | M5 from Gilmore model |

luminous dwarfs have a scale height of 90 pc. The faintest and older dwarfs have some maximum scale height $Z_{H,\text{disk}}^{\text{max}}$, taken by most workers to be 325 pc. For intermediate absolute magnitudes (M),

$$Z_{H,\text{disk}}(M) = Z_{H,\text{disk}}^{\text{max}} - (5.0 - M)(Z_{H,\text{disk}}^{\text{max}} - 90 \text{ pc})/3.0,$$

where $Z_{H,\text{disk}}(M)$ is constrained by $90 \text{ pc} < Z_{H,\text{disk}}(M) < Z_{H,\text{disk}}^{\text{max}}$. Disk giant stars are modeled as a population with a variable scale height usually near 250 pc. However, as noted by Reid & Majewski (1993), the giants' scale height has a negligible effect on star counts in high-latitude fields fainter than $V \approx 14$. For the disk luminosity function, we use Gilmore & Reid's (1983) fit to the solar neighborhood data (within 25 pc) from Wielen, Jahreiss, & Krüger (1983). This relation is well determined to $M_V \sim 13$. The luminosity function is allowed to decline after this (based on the faint luminosity function results of Tinney, Reid, & Mould 1993 and Tinney 1995). Even if this assumption were not true, the results on integrated star counts down to $O = 20$ is less than 2%. The disk also poses a special problem; for $-1.5 < M_V < 4$, a star can be either a giant or a subdwarf with different colors. Therefore, we adopt the relation derived by Gilmore (1981) for the fraction of stars that are main-sequence as a function of absolute magnitude. The color-magnitude relations for the main-sequence and giant populations are from the disk open cluster M67 (Chiu 1980).

3.2. The Halo

Among all of the Galaxy's populations, the halo is traditionally expected to have changed the least since it formed, and therefore it provides important clues to the Galaxy's formation and evolution. Eggen, Lynden-Bell, & Sandage (1962), in their classic paper, first proposed that the Galactic stellar halo formed rapidly during the collapse of a large protogalactic cloud. However, Searle & Zinn (1978) showed that many of the properties of the globular cluster population could be explained by the capture of many small protogalactic clouds during a much slower collapse. Neither of these models completely explains the kinematics and chemical composition observed in the stellar halo. Several recent discoveries have shown that the formation of the halo and the Galaxy was a complicated process. The distribution of stars in the halo and thick disk is less smooth than previously assumed, and mergers not only occurred during the Galaxy's formation but are still occurring today (the Sagittarius dwarf galaxy; Ibata, Gilmore, & Irwin 1995).

The halo is not only less massive than the disk (by a factor of 10), but it also occupies a much larger volume than the disk. As a result, the halo's stars do not combine their light effectively at large distances, which has made studies of the halos in other galaxies problematic. From studying photographic plates of nearby galaxies, de Vaucouleurs (1959) first proposed a projected surface brightness relation known as the $r^{1/4}$ law, which is two-dimensional. Poveda (1958) derived the full deprojected $r^{1/4}$ law, but it was mathematically cumbersome. Young (1976) found that for distances sufficiently removed from the core, a greatly simplified asymptotic form (for $R'/r_e > 0.2$) could be used:

$$D(r) = \frac{N_{\text{halo}}}{(R'/r_e)^{7/8}} \exp[-7.669(R'/r_e)^{1/4}],$$

where

$$R' = \sqrt{R^2 + Z^2}.$$

Here r_e , commonly known as the "de Vaucouleurs radius," is the radius from the center, R and Z are the Galactocentric coordinates, and N_{halo} is the ratio of halo to disk stars in the solar neighborhood. Some recent work has used a straight power-law model (Robin, Reylé, & Crézé 2000). We adopted the older effective-radius formulation for comparison with the earlier models, but the power law will be a useful approach for future work with the genetic algorithm. This relationship also assumes a perfectly round halo, which we now know is not correct (see Wyse & Gilmore 1989; Larsen & Humphreys 1994; Gould, Flynn, & Bahcall 1998; Yanny et al. 2000). Therefore, we handle the flattening of the halo in GALMOD through a linear transformation

$$Z \rightarrow (c/a)Z$$

in both R' and r_e , where c/a is the *axial ratio* of the halo.

We use Gilmore's luminosity function for the halo. On the bright end it is based on the luminosity function derived by Da Costa (1982) for 47 Tucanae, and at the faint end on the disk luminosity function. The two are smoothly joined at $M_V = +5$ with an adjustment for the blue horizontal branch. For the color-magnitude relation, we use the metal-poor globular cluster M5 (Sandage 1982).

3.3. The Thick Disk

Star-count studies established the existence of a new major component of the Galaxy, the thick disk. Although the excess of stars that would later be known as the thick disk was originally noted by Elvius (1965), it was not until the polar-cap star counts of Gilmore & Reid (1983) that the existence of this component gained widespread acceptance. The thick disk is probably similar in mass to the halo, but it is more disklike in shape. Its exact spatial distribution is not well known, but many external galaxies have surface density profiles that can be fitted by double-exponential thick disks. So, it is generally assumed (based on Gilmore & Reid 1983) to be similar to that of the disk. The density law is therefore

$$D(r) = N_{0,\text{thick}} \exp\left(\frac{-|Z - Z_0|}{Z_{H,\text{thick}}} - \frac{|R - R_0|}{R_{H,\text{thick}}}\right),$$

where $N_{0,\text{thick}}$ is the ratio of thick disk stars to disk stars in the solar neighborhood, $Z_{H,\text{thick}}$ is the scale height, and $R_{H,\text{thick}}$ is the scale length (usually assumed to be similar to that of the old disk).

The luminosity function for this component is also uncertain and is again modeled by assuming a similarity to the halo. The history of thick disk star formation is also unknown and is still a matter of discussion. Either the thick disk formed as an intermediate stage between the halo and the disk, or it may be the remnant of an ancient merger with another galaxy. In any case, it appears that insufficient gas remains to form new stars and the population has evolved like a globular cluster, although it is more metal-rich than most. We adopt the metal-rich globular cluster 47 Tuc as the typical color-magnitude relation for the thick disk (Sandage 1982; Cannon 1974; Harris, Hesser, & Atwood 1983).

A population of red horizontal-branch stars is associated with the thick disk and is included in GALMOD. The

enhancement factor used is the same as that for the halo. We add the extra stars but evenly distribute the colors in the range $0.70 < B-V < 0.90$.

3.4. Model Structure

The fundamental structure of GALMOD is its “distance loop.” Along any chosen direction, the distance from the observer to the observation point is allowed to increase in steps starting at 10 pc. The step size increases logarithmically—each distance step is $10^{0.02}$ times larger than the step before it. The volume added by the step is then calculated and is considered to be centered on the midstep distance (r_{mid}). This volume is filled with stars from the luminosity functions and color-magnitude relations as if the entire volume were situated at (l, b, r_{mid}) . After the last distance step (at 1 Mpc), the model terminates execution and outputs the resulting distribution of stars in the form of a color-magnitude diagram, $A(m_O, S_{O-E})$.

The density functions (Table 2) are defined relative to the Galactic center in a Galactocentric (cylindrical) coordinate system (R, Φ, Z) . One of the fundamental assumptions of Galactic modeling is that the Galaxy is axisymmetric (i.e., there is no Φ -dependence). A position in the Galactocentric coordinate system is therefore uniquely specified by its R and Z , and the Galactic populations are defined relative to the center at $R = 0$ and $Z = 0$. However, model star counts are calculated as a function of distance from the Sun in a given direction, (l, b) . Therefore GALMOD includes a geometric transformation from (r_{mid}, l, b) into R and Z .

It has been known for a long time that the Sun is displaced somewhat from the midplane of the Galactic disk, by a distance Z_\odot . The Bahcall & Soneira (1984) and Gilmore & Reid (1983) models ignore this for simplicity. Since GALMOD will be used for all-sky work, it must also be sensitive to Z_\odot . The principal effect of a nonzero Z_\odot is to incline the central plane of the disk and the Sun–Galactic center line of sight by an angle

$$\Theta = Z_\odot / R_\odot .$$

For even the extreme case of $R_\odot = 6000$ pc and $Z_\odot = 40$ pc, the angle is only $0^\circ 29'$ in the b -direction. However, the complete transformation required to appropriately transform (l, b, r_{mid}) to (R, Z) becomes computationally expensive. We use an approximation from Ratnatunga, Bahcall, & Casertano (1989) in which the Galactic center is moved Z_\odot above its true position as well. The plane and the Sun–Galactic center line are again aligned, and the transformation from r_{mid}, l , and b to Z simplifies to

$$Z = Z_\odot + r_{\text{mid}} \sin b .$$

The error introduced by this approximation is small. In addition, the magnitude of the error introduced decreases as one moves away from the Galactic center or anticenter direction.

The number of stars per magnitude is then determined using the volume, luminosity functions, and density functions. Calculations of the stars’ colors, corrections for interstellar extinction, and the stars’ expected apparent magnitudes are done during each distance step and are closely connected. The four color-magnitude relations used in GALMOD are included in the model as simple lookup tables. As described above, we have estimated the inter-

stellar reddening for each field using the maps of Burstein & Heiles (1982). The distribution of reddening in the Galaxy is patchy and can only be corrected statistically. Following both Gilmore and Bahcall & Soneira, we model the total amount of obscuration as an exponential with a 100 pc scale height centered on the Sun (regardless of the value of Z_\odot). At any Z -distance above or below the Sun’s position, the fraction of total reddening applied during the step [$E_{\text{step}}(B-V)$] is given by

$$E_{\text{step}}(B-V) = E(B-V) \left(1 - \exp \frac{|z|}{100 \text{ pc}} \right) .$$

The expected color for the stars is given by the color-magnitude lookup table and then reddened by adding $E_{\text{step}}(B-V)$. Fractional obscuration [$A_{\text{step}}(V)$] of the step is found via the universal extinction law. Finally, the expected apparent magnitude of the star is found via the standard distance formula. For comparison with the observed star counts, the magnitude (V) and color ($B-V$) from GALMOD are transformed onto the O and E passbands of the POSS I survey. The transformations used in the model are the same as those described in § 2.1.

The distribution $A(m_O, S_{O-E})$ predicted by GALMOD must also be corrected for *cosmic scatter* and measurement errors in the photometry. The cosmic scatter and photometric errors are computed only for the color coordinate and not the magnitude coordinate in $A(m_O, S_{O-E})$, because the expected error in apparent magnitude (m_O) is less than the bin size of the model (0.5 mag). In addition, brighter than $O = 20$ the derivative of the number counts with magnitude changes slowly enough that Malmquist-like effects are minimal. The color distribution, however, is quite susceptible to this scatter. Since the magnitude of the measuring error and cosmic scatter will vary from plate to plate, individual plate corrections were needed. During initial tests, we used GALMOD to predict a variety of color distributions between $O = 18$ and $O = 19$ with no error applied. For a large number of latitudes and longitudes, we found the predicted peak of the blue ridge in the color distribution had a full width at half-maximum (FWHM) of 0.1 mag. The width of the same peak in the POSS I data (σ_{data}) can be measured. Assuming the corrections are Gaussian, we can obtain an estimate of the dispersion needed by GALMOD (σ_{GALMOD}) through

$$\sigma_{\text{GALMOD}}^2 = \sigma_{\text{data}}^2 - 0.01 .$$

This dispersion is a function of magnitude, so for four POSS I fields, we measured σ_{data} for each magnitude bin. The four plates behaved similarly. The average width of the σ_{data} by magnitude was then scaled to the width of the $18 < O < 19$ bin. The FWHM between 18th and 19th magnitude was then measured for all of the fields. The Gaussian (σ_{GALMOD}) needed to “smear” the data as a function of magnitude was then stored as a model parameter.

In summary, we wrote GALMOD to achieve flexibility in dealing with large amounts of data and optimization for speed, a necessity for a large number of model calculations. It also includes, in the code, the binned star counts and the ancillary data for each field (e.g., positions, field reddening, estimated photometry errors, and completeness limits), which permits rapid modification. In addition, the star counts allow an internal calculation of goodness of fit via a χ^2 statistic between the data and computed model predictions.

4. THE GENETIC ALGORITHM

The goals of this study are to obtain a simultaneous and self-consistent set of global parameters that describe the shape of the Galaxy from our large, multifield and multi-directional data set and then to search for statistically significant deviations in the data when using these global parameters. Both require a method that impartially searches the parameter spaces and optimizes the match between the Galactic model and the observed star counts.

The optimization problem is formidable. We have 88 separate two-dimensional distributions that must be modeled using a seminumerical, multiparameter model, which is complicated by systematic and random noise, principally in the form of random photometric errors and zero-point shifts in the photometric calibrations. In addition, we have a strong suspicion that a single model or set of parameters will not adequately represent the observed distribution. There are several techniques that might be used to optimize the star-count model with the observed distributions (using a goodness-of-fit statistic), but most of the search techniques such as the familiar iterated search method have serious disadvantages for our Galactic model problem. For example, an iterated search will have a large execution time, and no history of the solution goes into the search; that is, a bad section of parameter space is searched as thoroughly as a good section.

We adopted the genetic algorithm technique for several reasons. Genetic algorithms use the paradigm of natural selection and “survival of the fittest” and were first rigorously described by Holland (1975). Essentially, a population of potential solutions randomly sampling the parameter space is created and assigned a fitness from the model. From these solutions, offspring are created. The technique is stochastic. However, each solution has a chance to contribute to these offspring proportional to its fitness, and less-fit solutions do not reproduce as often and so are removed from the population. The history of the population is used to guide new searches via evolutionary pressure, because the parameters of the parent solutions are used to create the offspring solutions. By favoring the fittest individuals in the population, the emphasis of the parameter-space search is on the most promising areas. Ease of implementation was a major factor in choosing this method as well, since the genetic algorithm requires no further knowledge about the problem than the range allowed for each parameter and the evaluation function (the Galactic model).

Although genetic algorithms have existed since the 1960s, they were only relatively recently introduced into other disciplines as an optimization method. Charbonneau (1995) provides a very good introduction to genetic algorithms for astrophysical applications and successfully applied them to three problems in astronomy: fitting galaxy rotation curves using four mass components (bulge, disk, dark halo, and gas), fitting multiple-periodic signals in the presence of noise and gaps, and fitting magnetohydrodynamic models containing multiple critical points. Their generality and robustness make genetic algorithms *slow*, and they are not necessarily the best technique for every problem. They are not guaranteed to find the absolute global maximum for a problem; however, the power of the genetic algorithm is in “finding ‘acceptably good’ solutions to problems ‘acceptably quickly’” (Beasley, Bull, & Martin 1993). In the Appendix, we provide some additional description of the

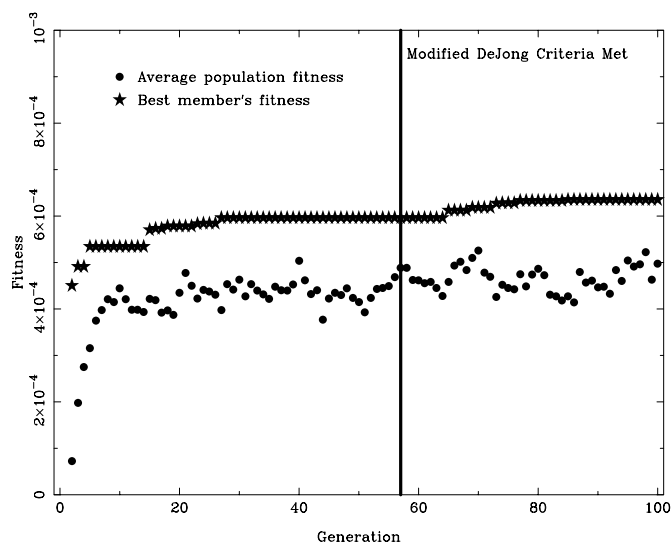


FIG. 6.—Fitness as a function of successive generations in a genetic algorithm, showing the average and best member of the population. The modified De Jong convergence criterion was met on generation 57. Note that since the genetic algorithm is elitist, the fitness of the best member of the population can never decrease because of removal from the population.

genetic algorithm and definitions of some of the terminology used with genetic algorithms.

The operation of a genetic algorithm is quite simple in concept; create a population of potential solutions, evaluate their fitness, and allow them through a process of selection and reproduction to populate the next generation. This process continues until convergence is reached or the maximum number of generations has passed. Figure 6 shows the evolutionary process for a single run of the genetic algorithm on our data. The axes show both average and best fitness of the population members as a function of generation. The genetic algorithm relatively rapidly evolves a population that approaches the fitness of the best-fit individual, and from then on, new mutations gradually improve the best member of the population even more.

4.1. The Genetic Algorithm and Galactic Model

One of the main advantages of the genetic algorithm is the ease with which it can be implemented. It was a simple matter to mate the APS data and GALMOD to the genetic algorithm. We used a code modified from a genetic algorithm written by D. Cormier and presented by Michalewicz (1994). The original version of the code had several errors that were detected and corrected in a test-bed version. Our Galactic model, GALMOD, is simply invoked in a subroutine, and the genetic algorithm–GALMOD combination is called GALG.

GALG has several standard properties of genetic algorithms. It is *elitist*, meaning that the most fit member of the population is never removed from the population. Individual members are allowed to reproduce according to their fitness. To ensure that premature convergence does not occur (a worry given our relative noisy data sets), the mutation rate is high (5% of all variables in all population members have values randomly mutated in a single generation). Normally, a genetic algorithm is considered to converge when 95% of the population reaches identical values for the parameters. This is known as the De Jong criterion (De Jong

1975). Our high mutation rate has the effect of reducing the level at which the population can conceivably converge, so GALG loosens the convergence criterion to be when 50% of the population reaches a single value for each parameter. GALG also uses a *steady state* or constant population size. The chance that a given member of the population dies and needs replacement by reproduction in any given generation is 30%. While this seems low, it allows good solutions to linger for a generation or two and reproduce before dying. In addition, the mutation rate will add additional new members to each generation.

Most importantly, GALG is a real-valued genetic algorithm. In theory, the most efficient genetic algorithms are binary-coded, since the binary representation of each model parameter defines an implicit Fourier sampling of its possible values. However, real-number encoding has produced similar and in some cases superior results in practice. The *building block* hypothesis of Goldberg (1991) states that should a chromosome be encoded so that related real-valued genes are close together, they also form an effective sampling of the available parameter space. The arrangement of the genes in GALG was chosen with Goldberg's hypothesis in mind. For example, our arrangement of genes creates the possibility that a superior disk fit may remain intact through crossover and perhaps join with a superior halo or thick disk fit to produce a superior overall fit. Goldberg concludes that the building block hypothesis works best when the real-valued genes contain little or no covariance. As noted by Beasley et al. (1993), however, we can almost always expect covariance between parameters in a genetic algorithm optimization. Without covariance, classical optimization techniques would prove more efficient.

Twelve of GALMOD's input parameters could vary (Table 3); in practice, however, convergence for all 12 parameters was very slow. For the purposes of this study, we chose to hold five of the parameters constant: the Sun's distance from the center and its distance above the plane, the density normalization of the disk, the scale height of the disk giants, and the maximum scale height of the disk. The ranges over which the other parameters were allowed to vary are also included in Table 3. Following the prescription of the building block hypothesis, GALG groups these parameters into four blocks: solar position, disk parameters, halo parameters, and thick disk parameters. When some of the 12 parameters are held fixed, the gene is shortened but the relative order of the variable parameters is not

changed. Under Goldberg's hypothesis, the parameters constituting a superior disk fit will statistically remain intact through crossover and perhaps join with a superior halo or thick disk.

4.2. The Fitness Function

The fitness function is critical to the success of a genetic algorithm. For GALG, the fitness function must represent the difference between the observed and modeled $A(m_O, S_{B-V})$ distributions. The function used by GALG is based on the χ^2 statistic:

$$\text{fitness}(\text{field}) = 2 \sum_{m_O, S_{O-E}} \frac{[A_{\text{field}}^{\text{model}}(m_O, S_{O-E}) - A_{\text{field}}^{\text{data}}(m_O, S_{O-E})]^2}{A_{\text{field}}^{\text{model}}(m_O, S_{O-E}) + A_{\text{field}}^{\text{data}}(m_O, S_{O-E})}$$

Note that this statistic makes the assumption that the errors in the distribution are Poissonian. However, the zero-point errors, combined with the nonuniformity of the actual counts, will not be well represented by this statistic. While we are using the χ^2 statistic to determine goodness of fit, the classic interpretation of the statistic is not valid here. The number of degrees of freedom was also computed with each determination of the statistic.

This statistic is computed for a given field only when more than five stars are in a given $A_{\text{field}}^{\text{data}}(m_O, S_{B-V})$ or $A_{\text{field}}^{\text{model}}(m_O, S_{B-V})$ bin, so that the denominators of the statistics are not zero. It is not computed or used fainter than the completeness limit given in Table 1 for each field, thus minimizing the chance that incompleteness in the counts has biased the fit.

GALG computes the individual fitness of each population member, as well as the total fitness of the population through a direct sum. The probability that a given population member will be selected in a given reproduction is the ratio of the member's fitness to the total population fitness.

5. GALACTIC MODEL RESULTS WITH THE GENETIC ALGORITHM

Thirty independent executions of the genetic algorithm were performed, using the computer resources of the APS lab, the University of Minnesota Laboratory for Computational Science and Engineering, the University of Minnesota School of Mathematics Scientific Computational Lab, and the University of Arizona's Spacewatch Project. Each execution took between 3 and 10 days, depending on the processor speed. We present the results of these computations in the following sections, separated by the assumptions in each case.

5.1. Test Case: Reproduction of an Artificially Created Noiseless Data Set

To check the general validity of the genetic algorithm for this problem, we first tested it against a noiseless model prediction of our Galaxy model. We adopted a set of parameters, those given in the "Original" line in Table 4, and used the Galaxy model of § 3 to create color-magnitude tables that were then presented to the genetic algorithm as the observational data to reproduce. We then ran the genetic algorithm six times to see how well it could reproduce the data.

TABLE 3
PARAMETER VALUES AND RANGES ALLOWED
IN OPTIMIZATION RUNS

| Parameter | Ranges and Values Allowed |
|--|---------------------------|
| Z_{\odot} | 20 pc |
| R_{\odot} | 8 kpc |
| $R_{H,\text{disk}}$ | 1.5–5.0 kpc |
| $N_{0,\text{disk}}$ | 1.00 |
| $Z_{H,\text{disk}}^{\text{max}}$ | 325 pc |
| $Z_{H,\text{disk,giants}}$ | 250 pc |
| N_{halo} | 0.0005–0.01 |
| r_e | 2–5.0 kpc |
| c/a | 0.45–1.2 |
| $R_{H,\text{thick}}$ | 1.5–5.0 kpc |
| $Z_{H,\text{thick}}$ | 800–1700 pc |
| $N_{0,\text{thick}}$ | 0.005–0.15 |

TABLE 4
BEST SOLUTIONS FROM TEST OPTIMIZATION WITHOUT NOISE

| Run | Fitness | $R_{H,disk}$ | c/a | r_e | $N_{0,halo}$ | $R_{H,thick}$ | $Z_{H,thick}$ | $N_{0,thick}$ |
|----------------|----------|--------------|-------|-------|--------------|---------------|---------------|---------------|
| 1..... | 51.8 | 3484 | 0.90 | 2030 | 0.0048 | 2721 | 1363 | 0.042 |
| 2..... | 48.1 | 3613 | 0.83 | 2562 | 0.0059 | 2344 | 1169 | 0.047 |
| 3..... | 74.8 | 3484 | 0.86 | 2625 | 0.0054 | 2403 | 1111 | 0.055 |
| 4..... | 13.3 | 3323 | 0.81 | 2262 | 0.0060 | 2518 | 1251 | 0.042 |
| 5..... | 660.9 | 3493 | 0.90 | 2616 | 0.0052 | 2449 | 1153 | 0.051 |
| 6..... | 72.2 | 3684 | 0.94 | 2878 | 0.0048 | 2390 | 1101 | 0.057 |
| μ | ... | 3514 | 0.87 | 2496 | 0.0054 | 2470 | 1191 | 0.049 |
| σ | ... | 114 | 0.04 | 276 | 0.0004 | 124 | 91 | 0.005 |
| Original | ∞ | 3500 | 0.90 | 2500 | 0.0050 | 2500 | 1200 | 0.050 |

Table 4 shows the results of the six trials meeting our modified De Jong convergence criterion. While our fitness statistic would explode if we exactly reproduced the input parameters, the random nature of the genetic algorithm, combined with its real encoding, practically guarantees that this would never happen. In all six cases we produce results very close to the “Original” parameters. The table gives the average (μ) and standard deviation (σ) of our six trials and clearly shows that every parameter was recovered in multiple trials to within 1σ .

We conclude from this that if our model were perfectly correct and that if our data were free of observational systematic effects, we would be able to use this technique to fit the Galaxy model and recover its basic parameters. We note that this test suggests that the hardest to recover parameters are c/a and the normalization of the halo to the solar neighborhood.

5.2. Test Case: Reproduction of an Artificially Created Data Set with Noise

We can characterize the expected zero-point errors in our observational data from estimates of the formal error of the mean in our photometric calibrations. Scale errors are far more complicated to model (note the shape of the calibration curve in Fig. 2) and were therefore neglected for this test. We then applied randomly generated zero-point errors from a Gaussian distribution to the color-magnitude diagrams used in the previous test, and these “noisy” color-magnitude diagrams were presented to the genetic algorithm as the observational data to reproduce. It was again run six times to see how well it could recover the input parameters.

Table 5 shows the results of the six trials upon meeting our modified De Jong convergence criterion. The fitness

statistic is now much smaller than it was before, by 2 orders of magnitude, the entire difference being the difficulty of matching the model to the noisy data in a classical “ χ^2 ” sense. However, despite the lower fitness we still adequately recovered the “Original” parameters. The means and standard deviations show that most parameters were recovered within 1σ and all were recovered within 1.25σ .

We note from these tests that the highest fitness statistic attainable is apparently very sensitive to noise (2 orders of magnitude are lost through the introduction of small zero-point errors). However, it does retain its ability to distinguish between fit and unfit models. Indeed, examination of the early generations shows fitness values that are up to 8 orders of magnitude less fit than the eventual “best fit.”

5.3. Full Analysis of the 88-Field Data Set

For the first full analysis of the data, we ran the genetic algorithm on all 88 fields. Table 6 shows the results of six separate executions meeting our modified De Jong convergence criterion. Note that the fitness statistic is much lower than for the trials in the previous section, by another 2 orders of magnitude. This is most likely due to the introduction of scale errors, which we expect to be of the same size, and about as important, as the zero-point errors, and to the inadequacies of our model design in describing the true Galaxy as represented by the star counts.

Each parameter seems to be relatively clustered about mean values, implying that the genetic algorithm has truly found a global minimum in the parameter space. However, we note that the results for the de Vaucouleurs radius from these trials are peculiar. In every case except one, it appears that the genetic algorithm is attempting to ascribe the largest possible value allowed for this parameter (5.0 kpc; see Table 2). The implication appears to be that the latitude

TABLE 5
BEST SOLUTIONS FROM TEST OPTIMIZATION WITH NOISE

| Run | Fitness | $R_{H,disk}$ | c/a | r_e | $N_{0,halo}$ | $R_{H,thick}$ | $Z_{H,thick}$ | $N_{0,thick}$ |
|----------------|----------|--------------|-------|-------|--------------|---------------|---------------|---------------|
| 1..... | 0.664 | 3885 | 0.85 | 2694 | 0.0057 | 2273 | 1146 | 0.049 |
| 2..... | 0.854 | 3471 | 0.92 | 2398 | 0.0049 | 2563 | 1204 | 0.050 |
| 3..... | 0.537 | 3395 | 0.79 | 2236 | 0.0062 | 2452 | 1241 | 0.044 |
| 4..... | 0.643 | 3414 | 0.83 | 2038 | 0.0054 | 2617 | 1358 | 0.042 |
| 5..... | 0.725 | 3599 | 0.84 | 2213 | 0.0055 | 2510 | 1242 | 0.047 |
| 6..... | 0.732 | 3632 | 0.86 | 2736 | 0.0055 | 2356 | 1171 | 0.050 |
| μ | ... | 3566 | 0.85 | 2385 | 0.0055 | 2461 | 1227 | 0.047 |
| σ | ... | 168 | 0.04 | 255 | 0.0004 | 118 | 68 | 0.003 |
| Original | ∞ | 3500 | 0.90 | 2500 | 0.0050 | 2500 | 1200 | 0.050 |

TABLE 6
THE FULL 88-FIELD FIT

| Run | Fitness | $R_{H,disk}$ | c/a | r_e | $N_{0,halo}$ | $R_{H,thick}$ | $Z_{H,thick}$ | $N_{0,thick}$ |
|----------------|----------|--------------|-------|-------|--------------|---------------|---------------|---------------|
| 1..... | 0.000534 | 4207 | 0.46 | 4965 | 0.0030 | 4236 | 812 | 0.031 |
| 2..... | 0.000530 | 3238 | 0.48 | 4995 | 0.0031 | 4764 | 855 | 0.023 |
| 3..... | 0.000603 | 3582 | 0.53 | 3374 | 0.0026 | 4998 | 907 | 0.024 |
| 4..... | 0.000645 | 3227 | 0.49 | 4780 | 0.0030 | 4789 | 812 | 0.029 |
| 5..... | 0.000639 | 3386 | 0.46 | 4662 | 0.0033 | 4833 | 952 | 0.018 |
| 6..... | 0.000628 | 3523 | 0.52 | 4970 | 0.0024 | 4713 | 891 | 0.028 |
| μ | ... | 3527 | 0.49 | 4624 | 0.0029 | 4722 | 872 | 0.025 |
| σ | ... | 331 | 0.03 | 571 | 0.0003 | 234 | 51 | 0.004 |

effects of the model’s halo component are ignored by the genetic algorithm to force a fit at the lowest Galactic latitudes.

To search for the cause of the poor fit for this parameter, we used the ratio of the observed number of stars to the number predicted by the model. A map of the ratios of observed to predicted stars for each field as a function of position on the sky is shown in Figure 7. Immediately obvious in the figure is a large overprediction by the model for the southern hemisphere compared with the north. Further examination shows relatively good matches to the lower latitude fields and poor fits to the fields at high latitudes and near the north Galactic pole. The good fits at the low latitudes may be driving the optimization and thus have led to the biases against the higher latitude fields. This is not surprising. The lower fields ($|b| \approx 20^\circ$) have the largest number of stars, the highest fraction of blended images, and the highest interstellar extinction, all of which could introduce uncertainties in the star counts. In our next test, we delete the lowest latitude fields, those with plate centers near $|b| \approx 20^\circ$.

5.4. Analysis of 79 Fields, $|b| > 20^\circ$

For our second experiment, we ran the genetic algorithm only on the 79 fields with $|b| > 20^\circ$. Table 7 presents the results of six trials meeting our modified De Jong convergence criterion. The mean value for the de Vaucouleurs

radius is lower, although some of the trials still give a result near the maximum allowed value. Examination of Figure 8, a plot on the sky of the observed-to-predicted ratios, shows that overall there is a much better fit, although a few of the fields show a significant excess of star counts. We note that the excess in the counts we reported (Larsen & Humphreys 1996) in the first quadrant of the Galaxy ($l = 20^\circ - 45^\circ$), when compared with the complementary fields in the fourth quadrant, shows quite clearly in Figure 8. Both the 88- and 79-field analyses yield rather large scale lengths for the thick disk (Tables 6 and 7). This result and its implications are discussed in § 6.

5.5. 79-Field Analysis with Fixed Axial Ratio

The thick disk and inner oblate halo predict stars in the same color and magnitude ranges; thus, the parameters describing these populations are covariant. To minimize the effects of this covariance, we used the previous observational result from § 1 and fixed the axial ratio of the halo at $c/a = 0.6$. Table 8 presents the results of six runs meeting our modified De Jong convergence criterion.

Our results for the thick disk are similar to the two previous experiments in many respects, but fixing the additional parameter forces the model to search the surrounding parameter space to compensate for the loss of a degree of freedom. The principal difference from the two previous tests is a much lower value for the de Vaucouleurs radius. Comparison of the model with the observed star counts

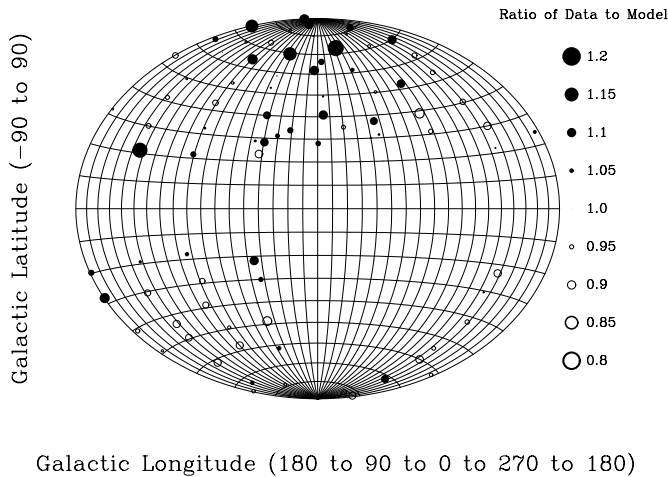


FIG. 7.—Aitoff projection showing deviation of the model from the data as seen in integrated counts for the 88-field fit. Note the large overpredictions in the southern Galactic hemisphere compared with the general underpredictions in the northern hemisphere.

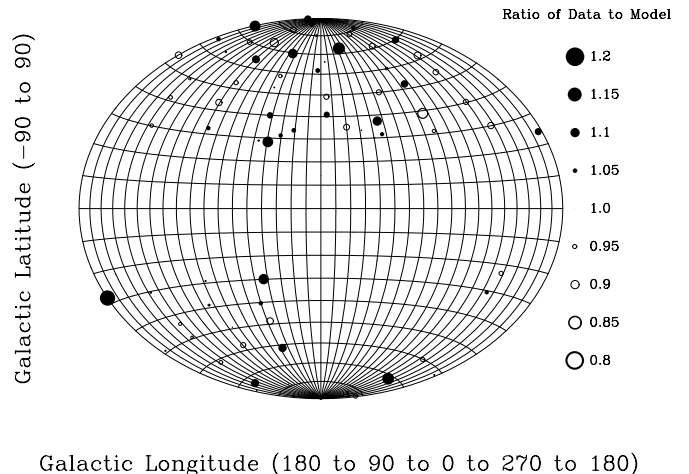


FIG. 8.—Same as Fig. 7, but for the 79-field fit. The mix of underpredictions and overpredictions indicates that we are closer to a true fit than in the 88-field case.

TABLE 7
FIT TO FIELDS WITH $|b| > 20^\circ$

| Run | Fitness | $R_{H,disk}$ | c/a | r_e | $N_{0,halo}$ | $R_{H,thick}$ | $Z_{H,thick}$ | $N_{0,thick}$ |
|----------------|----------|--------------|-------|-------|--------------|---------------|---------------|---------------|
| 1..... | 0.000610 | 3202 | 0.52 | 3134 | 0.0027 | 4888 | 823 | 0.031 |
| 2..... | 0.000614 | 3239 | 0.51 | 3483 | 0.0026 | 4346 | 915 | 0.025 |
| 3..... | 0.000635 | 3619 | 0.50 | 4897 | 0.0025 | 4840 | 930 | 0.024 |
| 4..... | 0.000635 | 3437 | 0.51 | 4854 | 0.0027 | 4854 | 904 | 0.022 |
| 5..... | 0.000598 | 4142 | 0.61 | 4728 | 0.0014 | 4728 | 1091 | 0.024 |
| 6..... | 0.000583 | 3331 | 0.65 | 4777 | 0.0014 | 4777 | 912 | 0.040 |
| μ | ... | 3495 | 0.55 | 4336 | 0.0022 | 4739 | 929 | 0.028 |
| σ | ... | 320 | 0.06 | 737 | 0.0006 | 183 | 80 | 0.006 |

(Fig. 9), however, shows poorer agreement, in which the model overpredicts the star counts over much of the sky. For this reason, in the next section we will focus the discussion and comparison on our results from the 88- and 79-field analyses with all seven parameters.

6. DISCUSSION OF MODEL RESULTS AND COMPARISON WITH PREVIOUS WORK

The Galactic parameters we derived in our different experiments with a genetic algorithm represent “global fits” using statistically significant star counts from fields distributed uniformly over most of the sky. These global all-sky fits will therefore not be significantly affected by tidal streams and the debris field that may be left by recent mergers (Majewski et al. 1999; Yanny et al. 2000; Martínez-Delgado et al. 2001), which may alter the star counts and especially the color distribution over relatively small spatial regions. Small pencil-beam surveys can identify interesting substructure in the local environment, but they cannot be used to determine the parameters that describe the Galaxy on a large scale, one that integrates over the local deviations. Conversely, these all-sky global fits can be used as a template to identify deviant regions. We have already mentioned that the 79-field solution recovered the asymmetry in the star counts observed between several fields in the first and fourth quadrants of the Galaxy described in Larsen & Humphreys (1996).

In Figures 10 and 11, we show two examples, P103 and P377, in very different directions on the sky, for which the comparison between the model-predicted color-magnitude diagram from the 79-field optimization and the observations is very good. In contrast, Figure 12 shows an example of a very deviant field, P498, for which the model grossly underpredicts the observed color-magnitude distribution for the faintest bins. This is one of the most deviant fields

found in Figure 8, yet the general trends of the model track the behavior of the star counts.

Most of the derived parameters in both the 88- and 79-field experiments are close to the nominal values expected from previous studies and models. The two parameters that differ the most from what may be called “expected” values are the radial scale length of the thick disk and the de Vaucouleurs radius. The parameters for our three modeled components of the Galaxy—halo, disk, and thick disk—and their implications are described separately below.

The halo.—All of the solutions yield a flattened axial ratio for the Galactic halo with $c/a \approx 0.5$ – 0.6 , which is not surprising given that several independent studies have concluded that the halo is not spherical, with additional evidence (Hartwick 1987, among others) that the axial ratio may vary with distance, becoming more spherical in the outer parts. With completeness limits for our fields typically 19.5th to 20th magnitude in the blue, our star counts are not sampling the outer halo. Our derived parameters for the halo are therefore most applicable to the inner halo. The results for the normalization of the halo to the disk (0.2%–0.3%) are consistent with previous work (Bahcall & Soneira 1980; Gilmore 1984; Kerber, Javiel, & Santiago 2001). Most of our solutions yielded much higher values, $\approx 4.3 \pm 0.7$ kpc with a range from 3.1 to 4.9 kpc for the 79 fields, for the de Vaucouleurs radius than is normally adopted ($r_e \approx 2.7$ kpc) in standard models for the Galaxy. However, they are within the range of acceptable solutions found by Kerber et al. (2001) from analysis of faint stars in *HST* fields. Kerber et al. also rule out a flattened halo, but their models apply to much fainter stars and are therefore sampling stars in the outer halo. Our solutions support Galactic models with a flattened inner halo and a larger effective radius than has previously been used.

The disk.—Our mean result for the radial scale length of the disk (3.5 ± 0.3 kpc), as well as the results in all of the

TABLE 8
FIT TO FIELDS WITH $|b| > 20^\circ$ AND $c/a = 0.6$

| Run | Fitness | $R_{H,disk}$ | c/a | r_e | $N_{0,halo}$ | $R_{H,thick}$ | $Z_{H,thick}$ | $N_{0,thick}$ |
|----------------|----------|--------------|--------------|-------|--------------|---------------|---------------|---------------|
| 1..... | 0.000578 | 3714 | 0.60 (fixed) | 3489 | 0.0014 | 4976 | 1005 | 0.033 |
| 2..... | 0.000584 | 2980 | 0.60 (fixed) | 3419 | 0.0020 | 4947 | 974 | 0.025 |
| 3..... | 0.000586 | 3439 | 0.60 (fixed) | 3303 | 0.0018 | 4741 | 919 | 0.031 |
| 4..... | 0.000580 | 4683 | 0.60 (fixed) | 2904 | 0.0023 | 4992 | 839 | 0.034 |
| 5..... | 0.000577 | 3566 | 0.60 (fixed) | 3169 | 0.0017 | 4767 | 1026 | 0.025 |
| 6..... | 0.000586 | 3662 | 0.60 (fixed) | 3483 | 0.0018 | 4981 | 856 | 0.037 |
| μ | ... | 3674 | 0.60 (fixed) | 3294 | 0.0018 | 4901 | 936 | 0.031 |
| σ | ... | 511 | ... | 207 | 0.0003 | 104 | 71 | 0.005 |

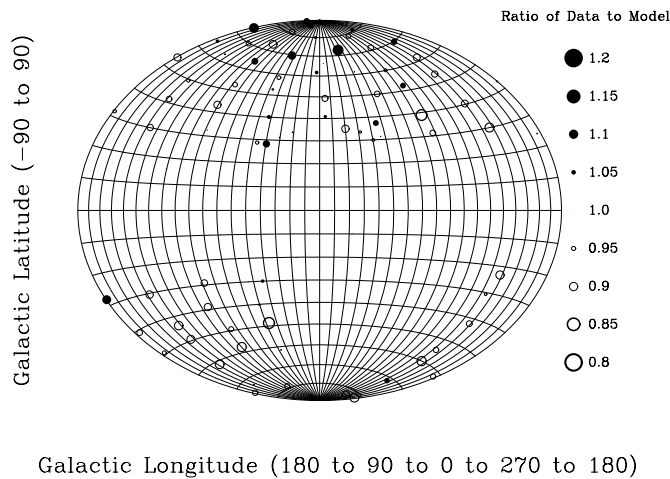


FIG. 9.—Same as Fig. 7, but for the 79-field fit with $c/a = 0.6$. This restriction seems to force the model into overpredicting for almost every field available to it.

separate trials, agrees remarkably well with the 3.5 kpc most often assumed in previous Galactic models based on optical star counts (Bahcall 1986; Gilmore 1984). However, our results do not support the much lower value (2.5 ± 0.3 kpc) derived by Robin et al. (1996) from midlatitude optical star counts alone or those from several studies using star counts in the near-infrared, which give values ranging from 2.6 to 2.0 kpc (Ortiz & Lépine 1993; Ruphy et al. 1996; Porcel et al. 1998), assuming R_{\odot} is 8 kpc. A fit to far- and near-infrared *COBE* DIRBE data (Drimmel & Spergel 2001) yielded a scale length of only $0.28R_{\odot}$, or approximately 2.2 kpc, although a recent analysis of 2MASS data by Ojha (2001) obtained 2.8 ± 0.3 kpc in a solution that also solved for the thick disk. In a recent study also using 2MASS data, López-Corredoira, Cabrera-Lavers, & Garzón (2002) showed that when the “flaring” or increase in scale height of the disk toward the Galactic center is included in the analysis, they derive a scale length of ~ 3.5 kpc for the old disk.

The thick disk.—Most previous star-count models for the thick disk yield either a high scale height (1.2–1.4 kpc) and low normalization (Gilmore 1984; Reid & Majewski 1993), or a lower scale height (700–900 pc) with higher normalizations, such as 4%–6% (see, e.g., Robin et al. 1996; Buser, Rong, & Karaali 1999). Our solutions for the thick disk are intermediate and favor a lower scale height of ≈ 900 pc ($870\text{--}930 \pm 50\text{--}80$ pc) with a normalization of only 2%–3%. Our results are most like Ojha’s (2001) for the thick disk from 2MASS data, except for our higher radial scale length of 4.7 ± 0.2 kpc compared with his value of $3.7^{+0.8}_{-0.5}$ kpc. In earlier Galactic models, such as Gilmore’s, the radial scale length of the thick disk has usually been set equal to that for the thin or old disk (≈ 3.5 kpc). Robin et al. (1996) have made an independent measurement of $R_{H,\text{thick}}$ using the same midlatitude star counts they used for the scale length of the disk. Their value of 2.8 ± 0.8 kpc is also lower than the nominal 3.5 kpc, but it is similar to their result for the scale length of the disk. Given that data from the same fields have been used for both, it is possible that they may not have corrected adequately for variable extinction along the line of sight. In contrast, our result for $R_{H,\text{thick}}$ not only is high, but more importantly, it is significantly different from the scale length of the disk. Buser et al. (1999) and Ojha

(2001) derive 3.0 ± 1.5 and $3.7^{+0.8}_{-0.5}$ kpc, respectively, and we note that Ojha’s value for the thick disk, like ours, is also significantly higher than his result for the old disk (2.8 ± 0.3 kpc). Recent work by de Grijs and collaborators (de Grijs & Peletier 1997) on edge-on disk galaxies has shown that disk galaxies may have both thick disk scale lengths and scale heights larger than for the dominant old disk. Although the origin of the thick disk is still uncertain, our results support models that treat it as a structure independent of the disk and perhaps with a very different origin.

When we compared the model-predicted star counts with the observations, we noticed that for many of the fields for which there was a significant discrepancy, the difference was greatest in the color range where the contribution from the thick disk would be greatest. For example, Figure 13 shows the comparison for P323, the north Galactic pole field. In this case, a better fit would require either a “thicker” thick disk, a higher scale height in this particular direction, or a redder color-magnitude diagram than 47 Tuc for the thick disk population. Other fields, P377, for example (Fig. 11), have a good match in the same color range. These results, combined with the large $R_{H,\text{thick}}$, suggest to us that the thick disk itself may be irregular or wavy with a scale height and density that are variable with direction. For example, compare Figure 13 for P323 with Figure 14 for P491. In the faintest magnitude ranges, while the blue and red peaks are adequately modeled, the thick disk is overpredicted in P323 and underpredicted in P491. Thus, the wide range of parameters in the literature for the thick disk may depend on where one is looking.

7. CONCLUDING REMARKS

The results from our first experiments with a genetic algorithm have demonstrated its validity and usefulness as a global optimization tool for Galactic models. Although we have used more data in the form of star counts and more complete sky coverage with a uniform data set than in previous models, we feel that our results are not necessarily the definitive answer but represent a first attempt to model an all-sky survey. Working with a photographic all-sky survey we had the advantage of sampling very large areas on the sky, but the results are limited both by a fairly bright completeness limit by modern standards, and by photometric error. However, the techniques described here will be valid for any of the large-scale digital surveys that are about to become available, such as the Sloan Digital Sky Survey (Chen et al. 2001). In particular, any large, contiguous survey could use a genetic algorithm to essentially “flat-field” their data. After applying the model, they could search for deviations in their counts that represent the myriad of asymmetries that could be expected in a spiral galaxy such as the Milky Way.

The genetic algorithm makes it extremely easy to add constraints on the data, which could take the form of data from much deeper pencil-beam surveys or surveys at other wavelengths that are more sensitive to the disk and not as prone to the uncertainties of interstellar extinction, such as the infrared. Improvements in the luminosity functions and the adopted color-magnitude relations can be easily added to the simple model presented here. The addition of kinematic data or results from kinematic studies can be used to narrow the parameter space to be searched and to refine the fitness of the solution to be consistent with the kinematic results.

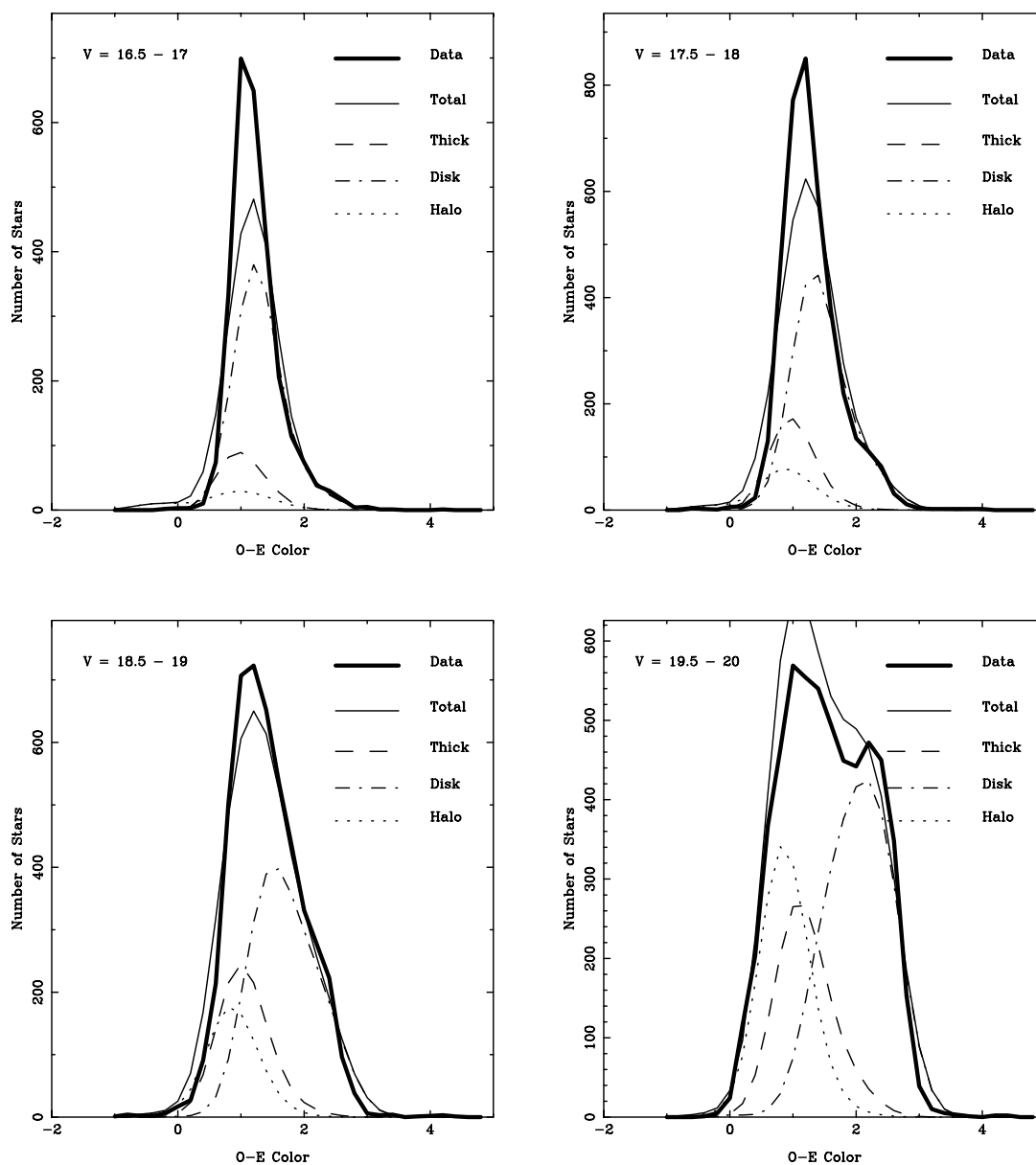


FIG. 10.—Examination of the model fit to the APS star-count data for P103 ($l = 88^\circ 7$, $b = 32^\circ 4$) under the 79-field optimization over several magnitude ranges.

The latter will be an interesting and important addition to future work with the genetic algorithm approach.

All-sky surveys are necessary for an understanding of the basic structure of the Galaxy. Pencil-beam surveys can penetrate very deep in small areas, but their results are limited to their local environment. This is especially true with the increasing evidence for Galactic mergers. The results we have presented here, while preliminary, already illustrate the advantage of an all-sky survey to leverage the results from a Galactic model, to obtain parameters that represent

the Galaxy as a whole, and to identify potentially deviant regions or directions for further study.

The authors are grateful to Fred Berendse for his assistance in developing and testing the first genetic algorithm code. We are also acknowledge gifts of computer time from the University of Minnesota's Laboratory for Computational Science and Engineering and the School of Mathematics Scientific Computational Laboratory, and from the University of Arizona's Spacewatch Program.

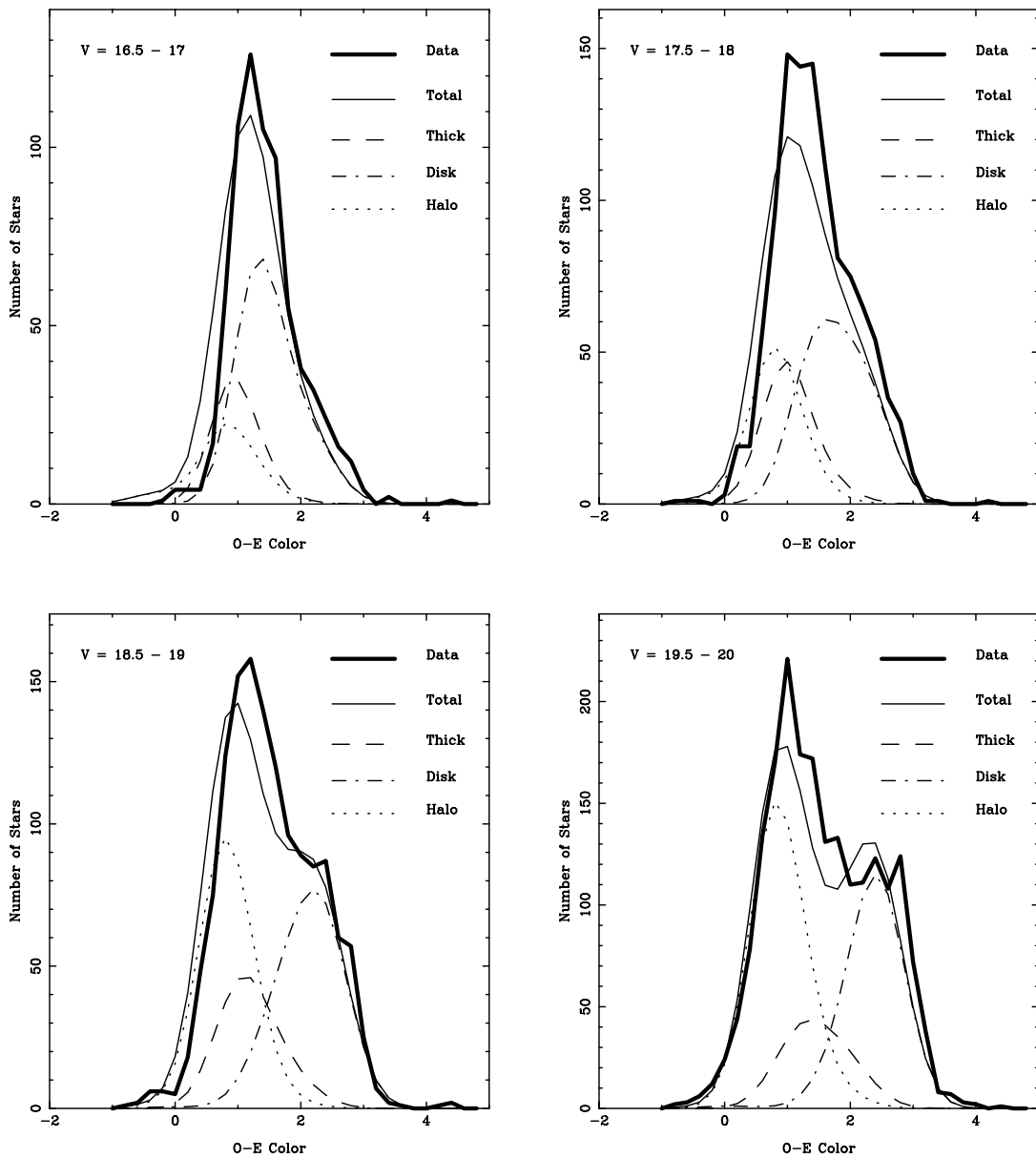


FIG. 11.—Same as Fig. 10, but for P377 ($l = 236^\circ.7$, $b = 80^\circ.9$). Note that although the model vs. data histograms are not perfectly aligned in color, the fitness statistic would assume the difference was a color zero-point error. This would normalize out photometry and reddening uncertainties to a certain extent.

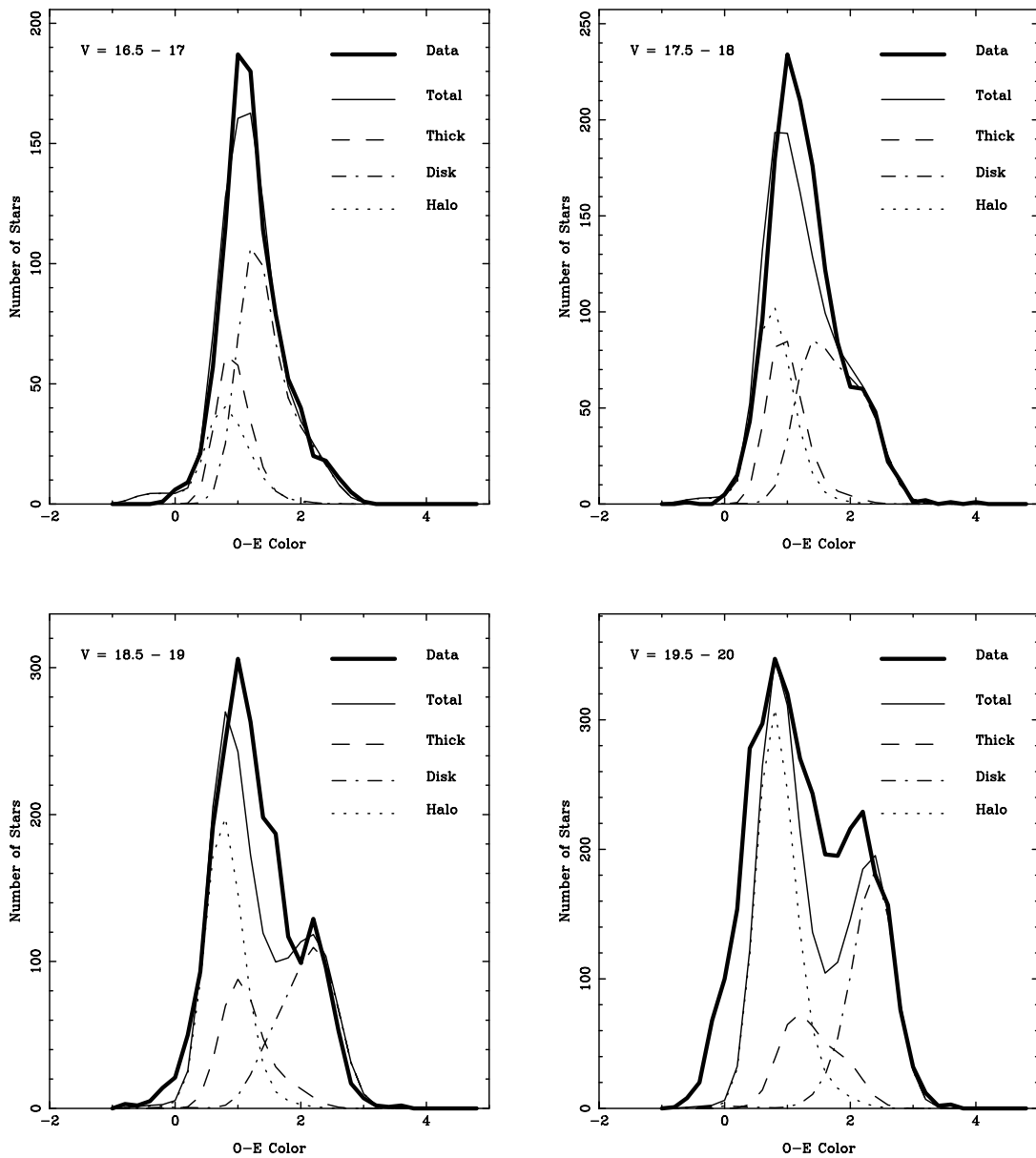


FIG. 12.—Same as Fig. 10, but for discrepant field P498 ($l = 326^\circ 6$, $b = 72^\circ 8$) under the 79-field optimization in several magnitude ranges. Note that the field is discrepant from its neighbors and the model grossly underpredicts the number of stars. Most probably, this field had a photometric scale error in the faint end of its calibration.

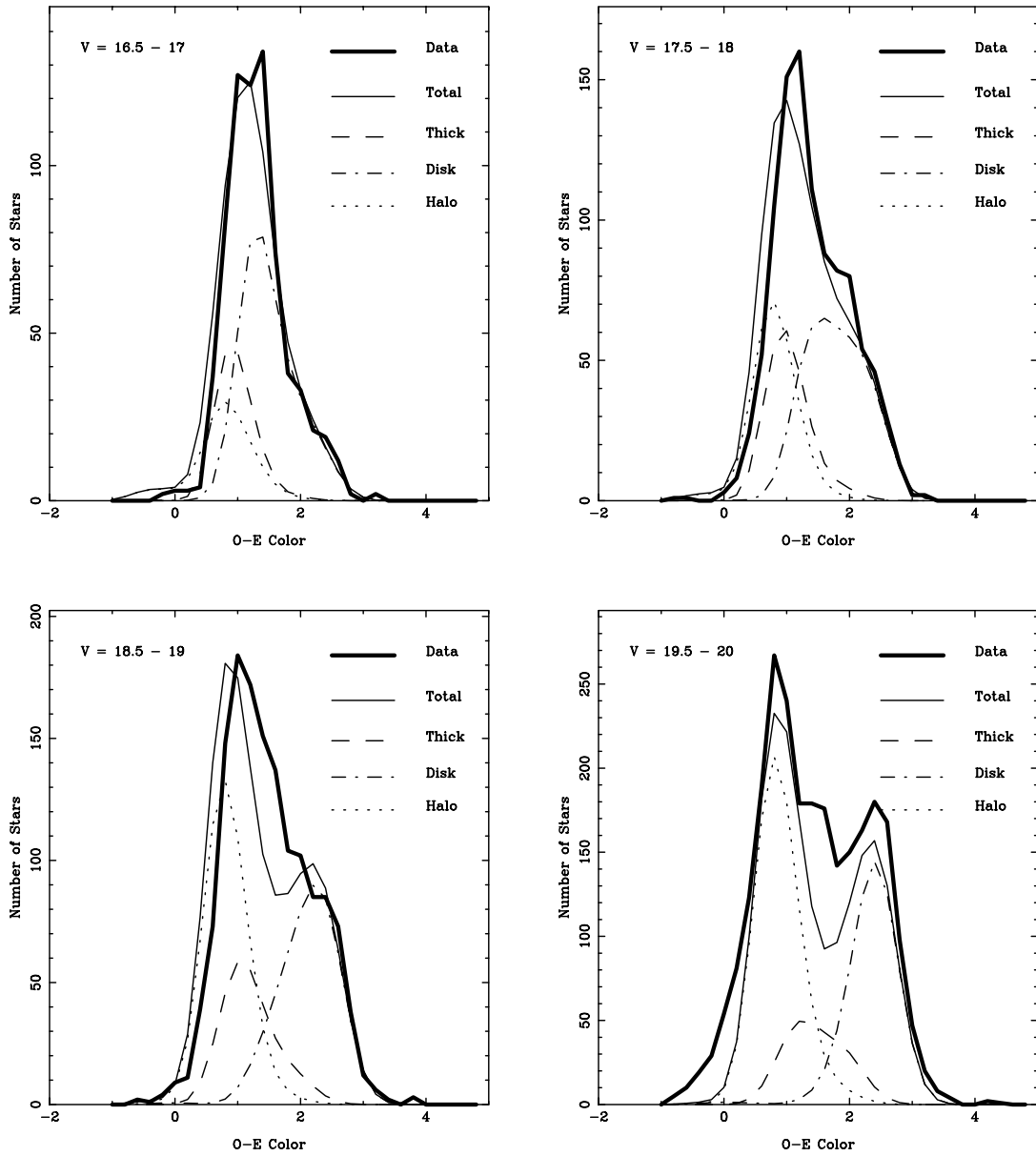


FIG. 13.—Same as Fig. 10, but for the north Galactic pole, P323 ($l = 65^\circ 4$, $b = 86^\circ 0$), under the 79-field optimization in several magnitude ranges. The thick disk does not adequately represent the color range $O-E \approx 1.0-2.0$ in the $O = 19.5-20.0$ bin, although other fields such as P377 (Fig. 11) seem to be adequately represented by the thick disk derived.

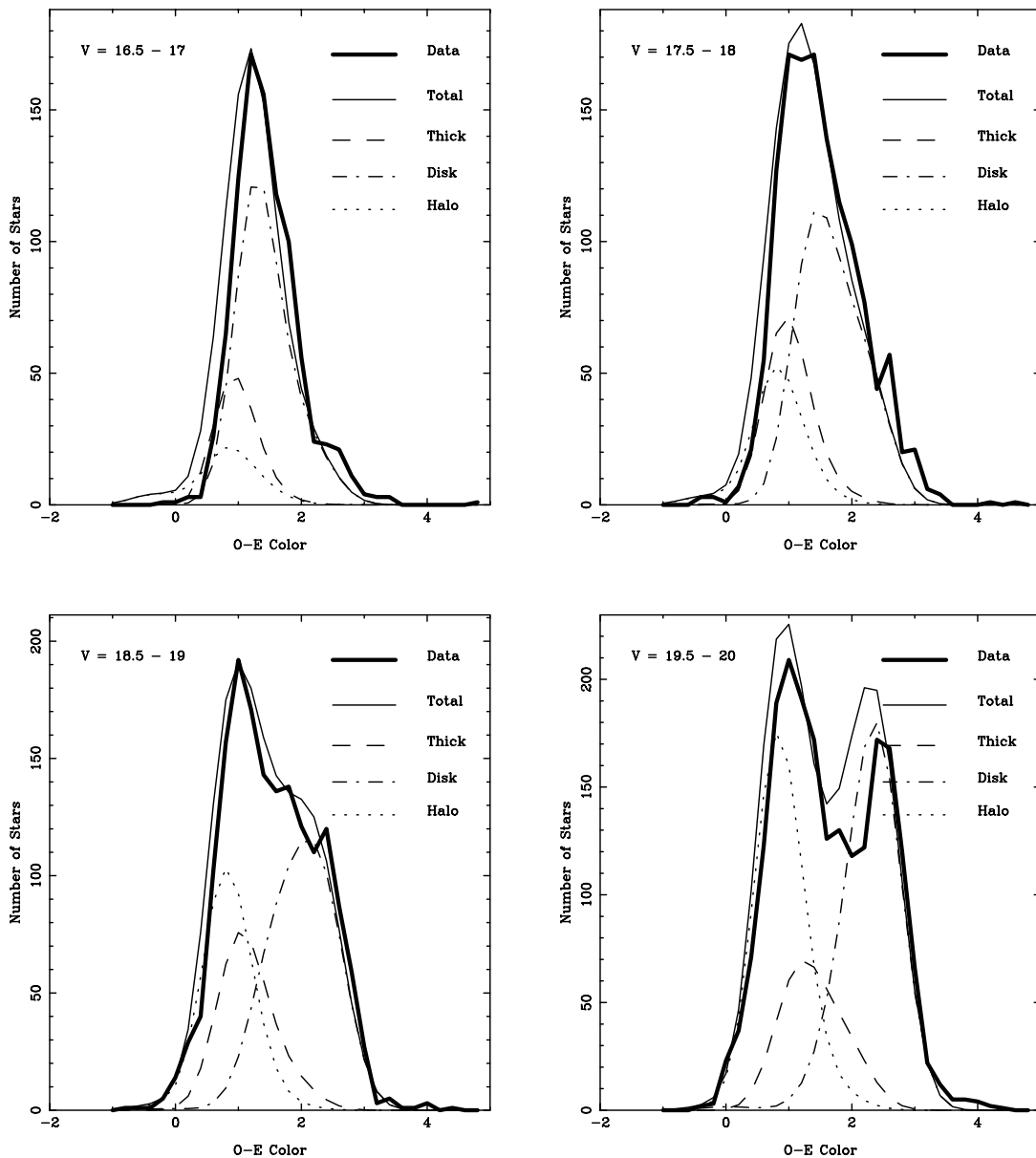


FIG. 14.—Same as Fig. 10, but for P491 ($l = 231^\circ 4$, $b = 54^\circ 0$) under the 79-field optimization in several magnitude ranges. Note that this field shows the opposite effect in faint mid-color ranges ($O-E \approx 1.0-2.0$) compared with P323 (Fig. 13). The applicability of any regular disk model for the thick disk may be in doubt.

APPENDIX

GENETIC ALGORITHMS

The basic principles of genetic algorithms have been around since the 1960s and were first rigorously described by Holland (1975). Several modern textbooks and papers are available for those who are interested in the details of the theory and application, including Michalewicz (1994), Charbonneau (1995), and Mitchell (1996). Here we give a brief summary of the explicit steps used by the genetic algorithm:

1. *Create a population of potential solutions.*—A genetic algorithm can be implemented for any multidimensional problem where the solution can be parameterized. In the parlance of evolutionary computing, each parameter is referred to as a *gene*. A set of parameters representing a pos-

sible solution to the optimization problem is called a *chromosome*. A *population* is a set of chromosomes that interact to form offspring. Alternately, a *genotype* refers to a chromosome and its values, while a *phenotype* refers to the “organism” created by the chromosome (in this application, the fitness of the Galaxy model using the parameters). In GALG, parameters in the initial solution are initially set to randomly selected values from the ranges given in Table 2.

2. *Obtain the fitness of each solution.*—Each phenotype is ranked by its fitness, a statistic describing how successfully it represented the data. The fitness is an arbitrary quantity, which in its roughest form is larger for a fit solution and smaller for an unfit solution.

Errors in the fitness function may manifest themselves in one of two ways. First, the fitness may be scaled badly, so that no individual has a clear advantage over another and

the genetic algorithm becomes essentially a random search. This type of error is referred to as *slow finishing*. On the other hand, the fitness may be so sharply weighted toward any improvement that *premature convergence* occurs for the first marginally good solution. In GALG, the fitness statistic is applied to each member of the population.

3. *Reproduction*.—Like all parents, genetic algorithms hope that by crossing two superior members of the population, the offspring will acquire favorable characteristics from both, becoming superior in the process. Every member of the population (except the most fit) has an equal chance to die (be removed) and be replaced through reproduction. The process of reproduction is facilitated through *crossover*, where the two parents are cut randomly along the chromosome and the tail end of one parent is joined to the beginning of the other. The method is formally referred to as *single-point crossover* and plays to maximize the effects of the building block hypothesis. GALG chooses parents using the fitness statistic discussed in § 4.2.

In addition, the population is kept viable through the introduction of *mutations*, random changes to a set number of parameters each generation. In general, mutations keep the solution from converging to a local maximum and stagnating by forcing occasional new solutions to be tried. Mutations add an element of random search to the genetic algorithm, although not quite enough to domi-

nate the process. GALG mutates 5% of all parameter values in all population members (except the most fit) each generation.

4. *Convergence*.—The genetic algorithm evolves over successive generations until the population begins to generally resemble the best-fit individual. De Jong (1975) formally defined convergence as the level at which 95% of the population has reached the same value for every gene. This is a very strict definition, however, and is not often reached in complex problems with a high mutation rate, as with GALG.

As described in the text, GALG is both elitist and real-valued. The real-valued parameters are numbers instead of the “purist” breakdown into binary representations. For example, a “pure” genetic algorithm would break down the number 137 into 10001001, and then crossover could occur within the value instead of between the values. This is described as an implicit Fourier sampling of the parameter space. We used Beasley et al.’s (1993) observation that the building block hypothesis arrangement of parameters on the chromosome was doing the same kind of sampling in “model” instead of “parameter” space and that empirically there was little real difference in results between real- and binary-coded parameter values when the parameters themselves are doing a Fourier-like sampling of the space.

REFERENCES

- Bahcall, J. N. 1986, *ARA&A*, 24, 577
 Bahcall, J. N., & Soneira, R. M. 1980, *ApJS*, 44, 73
 ———. 1984, *ApJS*, 55, 67
 Beasley, D., Bull, D. R., & Martin, R. R. 1993, *Univ. Comput.*, 15, 58
 Burstein, D., & Heiles, C. 1982, *AJ*, 87, 1165
 Buser, R., Rong, J., & Karaali, S. 1999, *A&A*, 348, 98
 Cannon, R. D. 1974, *MNRAS*, 167, 551
 Charbonneau, P. 1995, *ApJS*, 101, 309
 Chen, B., et al. 2001, *ApJ*, 553, 184
 Chiu, L.-T. G. 1980, *ApJS*, 44, 31
 Christian, C. A., Adams, M., Barnes, J. V., Butcher, H., Hayes, D. S., Mould, J. R., & Siegel, M. 1985, *PASP*, 97, 363
 Cunow, B. 1993, *A&A*, 268, 491
 Da Costa, G. S. 1982, *AJ*, 87, 990
 de Grijs, R., & Peletier, R. F. 1997, *A&A*, 320, L21
 De Jong, K. A. 1975, Ph.D. thesis, Univ. Michigan
 de Vaucouleurs, G. 1959, *Handb. Phys.*, 53, 311
 Drimmel, R., & Spergel, D. N. 2001, *ApJ*, 556, 181
 Eggen, O. J., Lynden-Bell, D., & Sandage, A. R. 1962, *ApJ*, 136, 748
 Elvius, T. 1965, in *Stars and Stellar Systems*, Vol. 5, Galactic Structure, ed. A. Blaauw & M. Schmidt (Chicago: Univ. Chicago Press), 41
 Evans, D. W. 1992, *MNRAS*, 255, 521
 Fleming, T. A., Liebert, J., & Green, R. F. 1986, *ApJ*, 308, 176
 Gilmore, G. 1981, *MNRAS*, 195, 183
 ———. 1984, *MNRAS*, 207, 223
 Gilmore, G., & Reid, N. 1983, *MNRAS*, 202, 1025
 Gilmore, G., Wyse, R. F. G., & Kuijken, K. 1989, *ARA&A*, 27, 555
 Goldberg, D. E. 1991, *Complex Syst.*, 5, 139
 Gould, A., Bahcall, J. N., Maoz, D., & Yanny, B. 1995, *ApJ*, 441, 200
 Gould, A., Flynn, C., & Bahcall, J. N. 1998, *ApJ*, 503, 798
 Harris, W. E., Hesser, J. E., & Atwood, B. 1983, *ApJ*, 268, L111
 Hartwick, F. D. A. 1987, in *The Galaxy*, ed. G. Gilmore & B. Carswell (NATO ASI Ser. C, 207) (Dordrecht: Reidel), 281
 Hartwick, F. D. A., & Schade, D. 1990, *ARA&A*, 28, 437
 Holland, J. H. 1975, *Adaptation in Natural and Artificial Systems* (Ann Arbor: Univ. Michigan Press)
 Humphreys, R. M., Landau, R., Ghigo, F. D., Zumach, W., & LaBonte, A. E. 1991, *AJ*, 102, 395
 Humphreys, R. M., & Larsen, J. A. 1995, *AJ*, 110, 2183
 Ibata, R. A., Gilmore, G., & Irwin, M. J. 1995, *MNRAS*, 277, 781
 Jarvis, J. F., & Tyson, J. A. 1981, *AJ*, 86, 476
 Kerber, L. O., Javiel, S. C., & Santiago, B. X. 2001, *A&A*, 365, 424
 King, I. R. 1971, *PASP*, 83, 199
 Koo, D. C., & Kron, R. G. 1982, *A&A*, 105, 107
 Kormendy, J. 1973, *AJ*, 78, 255
 Landolt, A. U. 1992, *AJ*, 104, 340
 Larsen, J. A., & Humphreys, R. M. 1994, *ApJ*, 436, L149
 ———. 1996, *ApJ*, 468, L99
 Lasker, B. M., et al. 1988, *ApJS*, 68, 1
 Liebert, J., Dahn, C. C., & Monet, D. G. 1988, *ApJ*, 332, 891
 López-Corredoira, M., Cabrera-Lavers, A., & Garzón, F. 2002, in *ASP Conf. Ser. 275, Disks of Galaxies*, ed. E. Athanassoula, A. Bosma, & R. Mujica (San Francisco: ASP), 127
 Majewski, S. R., Siegel, M. H., Kunkel, W. E., Reid, I. N., Johnston, K. V., Thompson, I. B., Landolt, A. U., & Palma, C. 1999, *AJ*, 118, 1709
 Martínez-Delgado, D., Aparicio, A., Gómez-Flechoso, M. A., & Carrera, R. 2001, *ApJ*, 549, L199
 McMahon, R. 1991, in *ASP Conf. Ser. 21, The Space Distribution of Quasars*, ed. D. Crampton (San Francisco: ASP), 129
 Michalewicz, Z. 1994, *Genetic Algorithms + Data Structures = Evolution Programs* (2d ed.; New York: Springer)
 Mitchell, M. 1996, *An Introduction to Genetic Algorithms* (Cambridge: MIT Press)
 Odewahn, S. C., Humphreys, R. M., Aldering, G., & Thurmes, P. 1993, *PASP*, 105, 1354
 Odewahn, S. C., Stockwell, E. B., Pennington, R. L., Humphreys, R. M., & Zumach, W. A. 1992, *AJ*, 103, 318
 Ojha, D. K. 2001, *MNRAS*, 322, 426
 Ortiz, R., & Lépine, J. R. D. 1993, *A&A*, 279, 90
 Parker, J. E., Humphreys, R. M., & Larsen, J. A. 2002, in *ASP Conf. Ser. 275, Disks of Galaxies*, ed. E. Athanassoula, A. Bosma, & R. Mujica (San Francisco: ASP), 136
 ———. 2003, in preparation
 Pennington, R. L., Humphreys, R. M., Odewahn, S. C., Zumach, W., & Thurmes, P. M. 1993, *PASP*, 105, 521
 Porcel, C., Garzón, F., Jiménez-Vicente, J., & Battaner, E. 1998, *A&A*, 330, 136
 Poveda, A. 1958, *Bol. Obs. Tonantzintla Tacubaya*, 2(17), 3
 Ratnatunga, K. U., Bahcall, J. N., & Casertano, S. 1989, *ApJ*, 339, 106
 Reid, N., & Majewski, S. R. 1993, *ApJ*, 409, 635
 Robin, A. C., Haywood, M., Crézé, M., Ojha, D. K., & Bienaymé, O. 1996, *A&A*, 305, 125
 Robin, A. C., Reylé, C., & Crézé, M. 2000, *A&A*, 359, 103
 Ruphy, S., Robin, A. C., Epchtein, N., Copet, E., Bertin, E., Fouqué, P., & Guglielmo, F. 1996, *A&A*, 313, L21
 Sandage, A. 1982, *ApJ*, 252, 553
 Schlegel, D. J., Finkbeiner, D. P., & Davis, M. 1998, *ApJ*, 500, 525
 Searle, L., & Zinn, R. 1978, *ApJ*, 225, 357

- Siegel, M. H., Majewski, S. R., Reid, I. N., & Thompson, I. B. 2002, ApJ, 578, 151
- Spiegel, D. N. 1992, in The Center, Bulge, and Disk of the Milky Way, ed. L. Blitz (Dordrecht: Kluwer), 77
- Tinney, C. G. 1995, ApJ, 445, 1017
- Tinney, C. G., Reid, I. N., & Mould, J. R. 1993, ApJ, 414, 254
- van der Kruit, P. C., & Searle, L. 1982, A&A, 110, 61
- Weinberg, M. D. 1992, ApJ, 384, 81
- Wielen, R., Jahreiss, H., & Krüger, R. 1983, in IAU Colloq. 76, The Nearby Stars and the Stellar Luminosity Function, ed. A. G. D. Philip & A. R. Uppgren (Schenectady: L. Davis), 163
- Wyse, R. F. G., & Gilmore, G. 1989, Comments Astrophys., 13, 135
- Yanny, B., et al. 2000, ApJ, 540, 825
- Young, P. J. 1976, AJ, 81, 807